CHAPTER-6

Formulation Development of Curcumin

6.1 Formulation Development

Formulations of CUR encapsulated lipopolysaccharide nanocarries and CUR encapsulated Eudragit E100 nanoparticles was prepared. Prepared formulations was optimized by using L_9 (3^4) Taguchi orthogonal experimental design as a systematic approach for mean particle size and percent entrapment efficiency. The optimized formulations were evaluated for physicochemical as well as solid state characterizations. Furthermore, the optimized formulations were evaluated for several *in-vitro* as well as *in-vivo* properties.

PART 1

6.1.1 Formulation, optimization and evaluation of CUR encapsulated lipopolysaccharide based nanocarriers (C-LPNCs) *in-vitro* and *in-vivo*

6.1.1.1 Preparation of physical mixture

The physical mixture (PM) in an equimolar ratio (1:1:1) was prepared manually by mixing CUR, soluthin MD® (SMD) and poloxamer 188 (PLX188) thoroughly for 10 min in a mortar and pestle until a homogeneous mixture was obtained. The sample was passed through 40# mesh and stored in a desiccator.

6.1.1.2 Preparation of C-LPNCs

The CUR loaded lipopolysaccharide nanocarriers was prepared by high speed homogenization technique as previously reported by Noack *et al.* (2001) with little modification. Briefly, CUR and SMD were dispersed in 15 ml distilled water containing 4%v/v ethanol and allowed to stir till complete solubilization of CUR and this forms as lipid phase. PLX188 was dissolved in 50 ml of distilled water followed by heating at 60-70°C to form aqueous phase. The lipid phase

subsequently added into aqueous phase under high homogenization speed (IKA® T25 digital ULTRA-TURRAX®, Germany) and stirred for 10 min to form C-LPNCs. Finally, the prepared formulations were stirred magnetically (IKA®, C-MAG, HS 7, Germany) for 24 hr, at room temperature to evaporate the residual organic solvent and allowed to form C-LPNCs. Further, the prepared formulations were centrifuged (Refrigerated Centrifuge RC 4100 F, Eltek, Mumbai, India) at 15000 rpm for 30 min. The sediment was washed, resuspended in distilled water containing 2% w/v mannitol as cryoprotectant and lyophilized (Freezeone, LABCONCO, USA). The lyophilized C-LPNCs were stored in glass vessels till further use. The method of preparation of C-LPNCs is schematically represented in Figure 6.1.

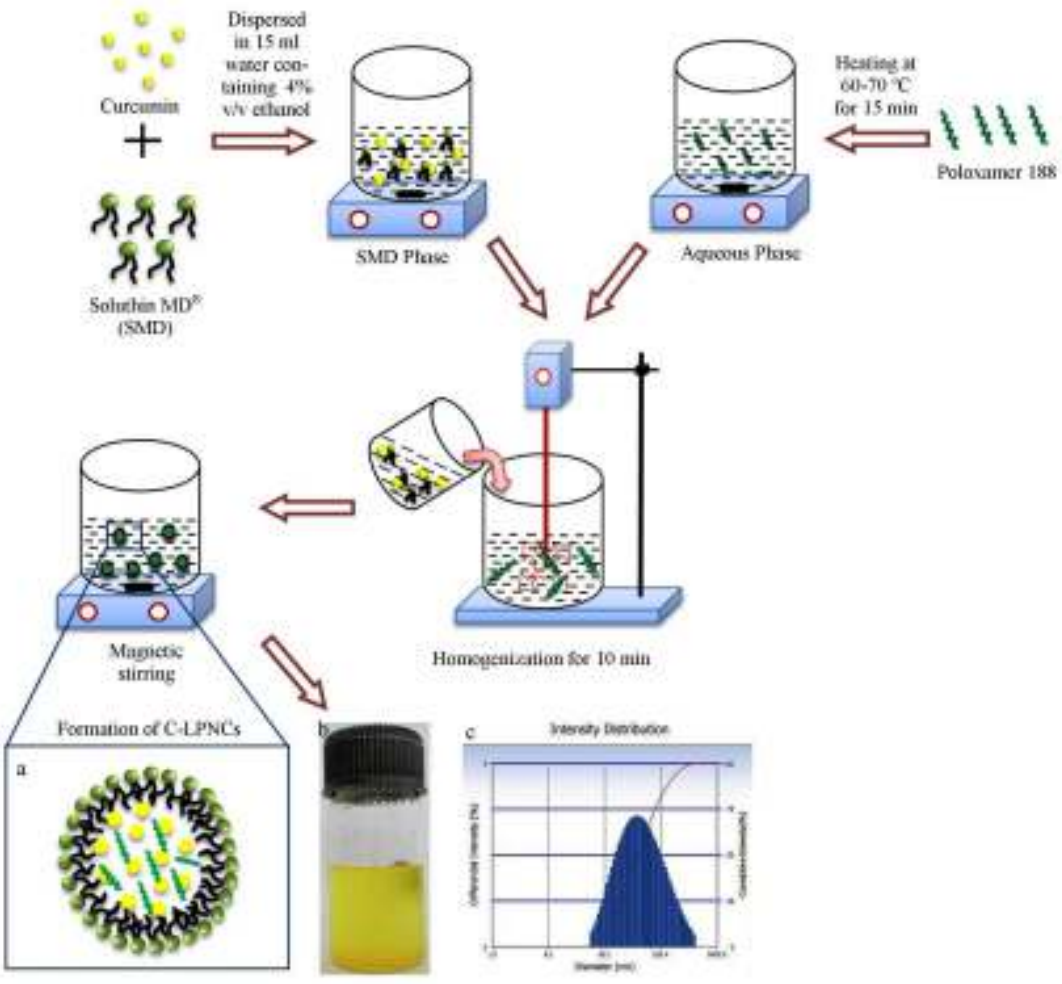

Figure 6.1 Schematic diagram showing (a) formation of C-LPNCs (b) aqueous dispersion of C-LPNCs and (c) particle size distribution

6.1.1.3 Characterization studies

6.1.1.3.1 Mean particle size, polydispersity index and zeta potential

The mean particle size (PS) and polydispersity index (PDI) were determined by using DELSA™ NANO C (Backman Coulter, Inc., USA) based on photon correlation spectroscopy by measuring the rate of fluctuations in laser light intensity scattered by particles as they diffuse through a dispersion. The intensity correlation functions were measured at 173°. The correlation functions were further analyzed using the cumulant approach as (Stepanek & Konak, 1984):

$$\ln g1\ (t) = \ln A - \Gamma t + \mu_2/2 \times t^2$$

Where, in A is the amplitude of the correlation functions, Γ is the decay rate and in a sufficiently diluted system it is related to the diffusion coefficient of the nanoparticles. The parameter μ_2 is the second-order cumulant which was used to compute the PDI.

PDI is dimensionless entity ($PDI=\mu_2/\Gamma^2$), which is a measure of the width of the monomodal decay rate distribution with values lying between 0 to 1 (0 value for monodispersed particles) (Oliveira *et al.,* 2013). Briefly, C-LPNCs was diluted with MilliQ water and analysed at 25°C for measurement of the PS and PDI.

The zeta potential (ZP, ζ) was determined based on electrophoretic light scattering by measuring the electrophoretic movement of charged particles under the influence of an applied electric field. The ZP of nanoparticles was also determined by the same instrument at 25°C using the above protocol. The C-LPNCs were placed in photoelectric cell; the movement within the electric field allows us to determine their electric charge (Kheradmandnia *et al.,* 2010). The ZP of the nanoparticles was determined by measuring their electrophoretic mobility (U_E) and the values were converted to ζ-potential (mV) through the Henry's equation:

$$\zeta = \frac{3\eta U_E}{2\varepsilon f(k_a)}$$

Where in η is the viscosity and ε is the dielectric constant of the medium. The parameter f(k_a) is the Henry's function which has been calculated through the Smoluchowski approximation f(ka)=1.5.

6.1.1.3.2 Entrapment efficiency (EE) and drug loading (DL)

%EE and %DL of C-LPNCs was estimated by using direct method. Briefly, C-LPNCs were centrifuged at 15,000 rpm for 15 min at 4°C to separate the C-LPNCs from the unentrapped drug. The supernatant was removed and 1 ml of PBS, pH 7.4 was added to the sediment and sonicated for 30 min at 80% amplitude using probe ultrasonicator (UP50H, Hielscher, USA) to break the nano structure for release of entrapped CUR. The suspension was filtered through 0.2 µm syringe filter. The filtrate was analysed for CUR on UV-Visible spectrophotometer (UV-Visible 1800, Shimadzu, JAPAN) at wavelength 420 nm. The %EE and %DL of C-LPNCs was calculated according to the following equations (Singh *et al.,* 2010):

$$\%EE = \left(\frac{amount\ of\ CUR\ encapsulated}{total\ amount\ of\ CUR\ used} \right) \times 100$$

$$\%DL = \left(\frac{amount\ of\ CUR\ loaded}{total\ amount\ of\ the\ prepared\ \ formulations} \right) \times 100$$

6.1.1.4 Design of experiment and statistical analysis

6.1.1.4.1 Software

Minitab® 16.2.1.0 (full version, Minitab Inc., USA) for automatic design of experiment using Taguchi Orthogonal Experimental Design (TOED) and statistical analysis was used in the present study. This software is equipped to use L_9 (3^4) arrays along with selection of four factors with three levels to each factor. The automatic design option allows Minitab® 16.2.1.0 to select the array used and assign factors to the appropriate columns.

6.1.1.4.2 TOED and crossed array layout

A L_9 (3^4) TOED (Taguchi, 1986; Rao *et al.,* 2008) was used in the current study to define the optimal conditions regarding the selected independent factors to produce nanoparticles with minimal PS, high %EE and required ZP. The robust design used to examine four independent factors each in three levels as shown in Table 6.1. The L and subscript 9 denote the Latin square and the number of the experimental runs, respectively. A run involved the corresponding combination of levels to which the factors in the experiment were set. The factors were amount of CUR, SMD concentrations, PLX188 concentrations and homogenization speed. As shown in Table 6.2, the L_9 (3^4) array had 9 rows and four columns at three levels. Each of the nine experiments was performed in triplicate, corresponding to a total of 27 tests to reduce experimental errors (Waddada *et al.,* 2013). Three major tools used in the Taguchi method are the orthogonal arrays, analysis of variance and the mean response/signal-to-noise ratio(S/N).

In the application of robust design, Taguchi method defines two types of variables or factors in the system: control factors and mean/noise factors. A control factor can be selected and fixed at a certain level. On the contrary, a mean/noise factor can not be controlled because of practical, economic, or other reasons (Taguchi, 1986).

Taguchi method constitutes an effective tool for selecting the best combination of levels of control factors of a system to obtain a combination of factors that enable a robust behavior against the variation of mean/noise factors (Mousavi *et al.,* 2007). A robust solution is the combination of factors whose variation does not produce a sensible change in the response.

Table 6.1 Independent factors and their corresponding levels of TOED (4-factors, 3-levels)

Independent Factors	Levels		
	Low (1)	**Medium (2)**	**High (3)**
A: Amount of Drug (mg)	5	10	15
B: SMD concentration (%w/v)	0.1	0.4	0.9
C: PLX188 concentration (%w/v)	1.0	1.5	2.0
D: Homogenization speed (rpm)	10000	12000	14000

Table 6.2 Taguchi L_9 (3^4) orthogonal Arrays

Batches	A	B	C	D
C-SMD1	5	0.1	1.0	10000
C-SMD2	5	0.4	1.5	12000
C-SMD3	5	0.9	2.0	14000
C-SMD4	10	0.1	1.5	14000
C-SMD5	10	0.4	2.0	10000
C-SMD6	10	0.9	1.0	12000
C-SMD7	15	0.1	2.0	12000
C-SMD8	15	0.4	1.0	14000
C-SMD9	15	0.9	1.5	10000

Where, A: amount of drug (mg); B: SMD concentration (%w/v); C: PLX188 concentration (%w/v); D: homogenization speed (rpm)

6.1.1.4.3 Analysis of Variance (ANOVA)

ANOVA can be useful for determining the influence of any given input parameter from a series of experimental results by TOED for nanoparticles formulation and it can be used to interpret experimental data (Lin & Lin, 2002). A concept may be represented that any high dimensional function may be broken down into subset of terms as:

$$f_{(X)} = f_o + \sum_{i=1}^{n} f_i(x_i) + \sum_{i=1}^{n}$$

$$\sum_{j=i+1}^{n} f_{i,j}(X_i, X_j) + f_{1,2,\ldots\ldots\ldots,n}(X)$$

Where n represents number of inputs f_o is a constant (bias term) on right hand side represent univariate, bivariate, trivariate, etc., functional combinations of input parameters.

ANOVA partitions total variation into its appropriate components. Total sum of squares term can be defined as

$$SS_T = \sum y_i^2$$

For i=1, 2,……n

This can be given as

$$SS_T = SS_m + SS_e$$

Where, $SS_m = nM^2$ and $SS_e = \sum (y_i - M)^2$ are mean sum of squares and error sum of squares respectively, with $M = 1/n \sum y_i (i = 1,2,\ldots\ldots,n)$.

In case of two-way ANOVA, when interaction effect of main factors affects output values, total variation may be decomposed into more components as

$$SS_T = SS_A + SS_B + SS_{AB} + SS_e$$

Where, $SS_A = (A_1 - A_2)$ and $SS_B = (B_1 - B_2)$ are variations due to factors A and B respectively, while $SS_{AB} = \sum (AB)i^2 / n_{ABi}$ for i=1, 2,……,k is variation due to interaction of factors A and B, where k represents number of possible combinations of interacting factors and n_{ABi} is number of data points under these conditions.

While performing ANOVA, degrees of freedom should also be considered together with each sum of squares. In ANOVA studies with certain pooled error, error variance determination is very important. Obtained data are used to

estimate F value of Fisher test (F-test). Variation observed (total) in an experiment attributed to each significant factor (p<0.05) or interaction is reflected in percent contribution (%PC), which shows relative power of a factor or interaction to reduce variation. Factors and interactions with substantial %PC play an important role. Therefore, the following formula uses to calculate %PC of each factor (Waddada *et al.,* 2013):

$$\%PC = \left(\frac{SS}{SS_{total}} \right) \times 100$$

6.1.1.5 Solid state characterization

6.1.1.5.1 Fourier transform infrared spectroscopy study

The pure CUR, SMD, PM and optimized C-LPNCs were characterized by using fourier transform infrared (FTIR) spectrophotometer (FTIR 8400S system, Shimadzu, Japan) to evaluate the possible chemical interactions, if any, between the drug and excipients. Briefly, the sample was crushed individually with dry potassium bromide in mortar and pestle followed by its compression into a pellet by using pressed pellet technique. The compressed pellet was placed in the FTIR sample holder and scanned in the absorbance mode between the spectral region 4,000 to 400 cm^{-1}using the resolution of 1 cm^{-1} to obtain FTIR spectra.

6.1.1.5.2 Differential scanning calorimetric study

The differential scanning calorimetric (DSC) analysis was done to study the state of drug inside the nanoparticles. The DSC thermograms of pure CUR, SMD, PM and optimized C-LPNCs was evaluated using Thermogravimetric Analyzer/Differential Scanning Calorimeter (STAR® System, Mettler Toledo, Switzerland). Each sample (approximately 2-5 mg) were crimped with a lid containing pin hole in aluminium pan and heated from 30 to 300°C at a scanning rate of 10°C/min in an atmosphere of nitrogen gas at 10 ml/min. An empty loosely covered aluminium pan was used as reference. The DSC was calibrated for baseline using indium as a standard.

6.1.1.5.3 Powder X-ray diffraction study

The Powder X-ray diffraction (*p*XRD) patterns of pure CUR, SMD, PM and optimized C-LPNCs were obtained using X'Pert Pro X-Ray diffractometer (PANalytical, Holland) with monochromatic Cu $K\alpha_1$ radiation (λ=1.54187 Å) generated at a voltage of 40 kV and 40 mA. The X-ray spectra were acquired at room temperature and diffractogarms were collected in transmission mode from 10°-50°, 2θ at a scan rate of 0.1° 2θ/min.

6.1.1.6 Morphological evaluation

6.1.1.6.1 High resolution transmission electron microscopy study

The surface morphology of the optimized C-LPNCs was studied using high resolution transmission electron microscopy (HR-TEM) (TECHNAI $20G^2$, FEI Company, Netherlands, Holland). The samples were prepared by spreading small drop of C-LPNCs dispersions onto a carbon-coated copper grid surface. After 1 min of adsorption, excess liquid was blotted off with filter paper and air dried at room temperature. The dried specimens were examined with HR-TEM at an acceleration voltage of 200 kV. Images were visualized and collected by soft imaging software.

6.1.1.6.2 Atomic force microscopy study

The shape and size distribution of optimized C-LPNCs was characterized by atomic force microscopy (AFM), SOLVER next (NT-MDT, Moscow, RUSSIA). A drop of the diluted C-LPNCs dispersions (1 mg/ml) was placed on freshly cleaved mica. After 5 min of incubation the surface was gently rinsed with deionized water to remove unbound C-LPNCs. The sample was air dried at room temperature and mounted on the microscope scanner. The shape was observed and imaged in noncontact mode with scanning rate 0.5 Hz.

6.1.1.7 Evaluation of drug distribution within the lipopolycassharide nanocarriers

The distribution of CUR within the lipopolycassharide nanocarriers (LPNCs) was examined by using confocal laser scanning microscope (CLSM 510 Meta, Carl Zeiss, USA). Since CUR is naturally fluorescent in the visible green spectrum, no further labeling of CUR was needed. A small drop of the C-LPNCs was mounted on a slide and air dried at room temperature before visualization in the green fluorescence excitation wavelength of 488 nm. Fluorescent, differential interference contrast (DIC) images and merge of fluorescent and DIC image were obtained.

6.1.1.8 Analysis of photophysical properties

Entrapment of CUR into the core of LPNCs was further examined by UV-Visible spectroscopic analysis (Sahu *et al.,* 2008). The absorbance spectra of both pure CUR and optimized C-LPNCs (both dissolved in PBS, pH 7.4) having concentration 3 µg/ml for the spectroscopic experiments. Aqueous optimized C-LPNCs dispersions were vortexed followed by sonication for 1 min (WUC 1.8L, Fisher Scientific, India) to get well dispersed solution for spectroscopic studies. CUR was quantified spectrophotometrically at 420 nm wavelength.

6.1.1.9 *In-vitro* drug release study

Dialysis bag diffusion technique was used to study *in-vitro* release of CUR from the prepared C-LPNCs in PBS, pH 7.4 (Verger *et al.,* 1998). The 3 ml of optimized formulation (equivalent to 2 mg of CUR) was placed in the dialysis bag (MWCO≥12 kDa, Sigma Diagnostics, USA), hermetically sealed and immersed into 100 ml of the PBS, pH 7.4 (containing 1% v/v Tween 80) as a release media maintained at 37±0.5°C under continuous stirring at 50 rpm. At specific time intervals (½, 1, 2, 3, 4, 5, 6, 7, 8 and 24 hr), 5 ml of aliquots were withdrawn from the medium and replaced with an equal amount of fresh pre-warmed (37±0.5°C) medium to maintain sink condition. The samples were filtered through 0.2 µm syringe filter and were analyzed spectrophotometrically at 420 nm wavelength.

The different release kinetic models: zero order, first order, Higuchi, Korsmeyer–Peppas and Hixon-Crowell were fitted to the experimental data to evaluate the drug release mechanism (Costa & Sousa, 2001).

$$Zero\ order; \quad \frac{\%R_t}{\%R_\infty} = k \times t$$

$$First\ order; \quad \frac{\%R_t}{\%R_\infty} = 1 - e^{-kt}$$

$$Higuchi's\ equation; \quad \frac{\%R_t}{\%R_\infty} = k \times (t)^{1/2}$$

$$Korsmeyer - Peppas\ equation; \quad \frac{\%R_t}{\%R_\infty} = k \times t^n$$

$$Hixon - Crowell\ \mathrm{mod}\,el; \quad W_0^{1/3} - W_t^{1/3} = k_s \times t$$

where $\%R_t$ is the percentage of drug released at time t, $\%R_\infty$ is the total percentage of drug released, $\%R_t/\%R_\infty$ is the fraction of drug released at time t, k is the release rate constant, n is the diffusion release exponent that could be used to characterize the different release mechanisms; $n \leq 0.5$ (Fickian diffusion), $0.5 < n < 0.85$ (anomalous transport), and $n \geq 0.85$ (case II transport, i.e., zero-order release). On the other hand, W_0 is the initial amount of drug, W_t is the remaining amount of drug at time t and K_s is a constant incorporating the surface-volume relation.

6.1.1.10 Stability study

Freshly prepared freeze dried powder sample of formulation was packed in amber colored glass vials, sealed and maintained at room temperature 25°±2°C/60%±5% standard relative humidity and at ambient conditions for a period of 3 months. The dried powder samples subjected for stability test were redispersed in distilled water and analyzed according to the above mentioned protocols. At various time points, the physical changes such as differences in PS, PDI and %EE was recorded. Moreover, *in-vitro* drug release behavior of the stored optimized formulation was compared with the freshly prepared batch as described above.

6.1.1.11 *In-vivo* pharmacokinetic study

6.1.1.11.1 Animals

The animal details are discussed earlier in ***Sub-section 4.1.3.1.***

6.1.1.11.2 Dosing and sampling

Albino Wister rats of either sex (weighed 200-250 g) were deprived of food but had free access to water 12 hr before the day of the experiment. The animals were divided into three groups comprising six animals in each, Group I and Group II received pure CUR and PM, dispersed in 0.3% sodium carboxymethylcellulose to form aqueous suspension, respectively whereas Group III received optimized C-LPNCs. All the groups received CUR (2 ml of aqueous suspension) equivalent to a dose level of 50 mg/kg body weight orally. At different time intervals (0.25, 0.50, 0.75, 1, 2, 4, 8 and 12 hr), rats were anesthetized using ether and blood samples (500 µl) were collected via retro-orbital plexus into heparinized microcentrifuge tubes (Meier *et al.,* 1974). Plasma was separated immediately after blood collection by centrifugation at 5000 rpm for 10 min at -4°C and stored at -20°C until analysis.

6.1.1.11.3 Chromatography conditions and drug extraction

The details of chromatography conditions and drug extraction are mentioned in ***Sub-section 5.1.1.3.1 and 5.1.1.3.3***, respectively.

6.1.1.11.4 Pharmacokinetic parameters

The pharmacokinetic parameters for all CUR formulations were determined with the help of "Kinetica 5 Trail Version" (PK/PD analysis, Thermofisher scientific) and compared with the pharmacokinetic data of pure CUR. The area under the plasma concentration-time curve ($AUC_{0\text{-}12h}$) was calculated using the linear trapezoidal method. The peak plasma concentration (C_{max}), time to reach the peak plasma concentration (T_{max}) and biological half life ($t_{1/2}$) were computed.

6.1.1.12 Cell culture experiments

6.1.1.12.1 Cells

The details of cells and their culture conditions are explained in ***Sub-section 4.1.3.2***.

6.1.1.12.2 *In-vitro* cytotoxicity study

Sulphorhodamine B (SRB) assay was used for *in-vitro* cytotoxicity screening which is based on the measurement of cellular protein content of adherent and suspension cultures in 96-well format (Vichai & Kirtikara, 2006). Colon-26 cells (1.9×10^4 cells/ml) were placed into 96 well plates and incubated at 37°C. After overnight growth, cells were treated with different concentrations of pure CUR suspension, PM and optimized C-LPNCs and were incubated in a humidified 5% CO_2 at 37°C for 24 hr. Untreated cells were used as control. 100 mg of CUR (test sample) was accurately weighed and dissolved in 1 ml of dimethyl sulphoxide (DMSO), diluted appropriately to 1 mg/ml. Further dilutions were made in sterile deionized water to get 0.1 to 100 µg/ml. The eight rows of 96-well culture plate were designated as A, B, C, D, E, F, G. 10 µl of the each test sample in 10% v/v DMSO in sterile deionized water was added to each compound well of a 96-well culture plate in rows B, C, D, E, respectively. 10 µl of 10% v/v DMSO was added into each negative control well in rows F and G. The cell monolayers were removed from the medium and washed with sterilized phosphate buffer pH 7.4. The mono-layer cell culture was trypsinized by adding 0.25% w/v trypsin in versene-EDTA (0.25 g EDTA and 1.5 ml of 0.5% w/v phenol red solution in 100 ml of phosphate buffer pH 7.4) and dispersed in10 ml of culture medium. The cell concentration was adjusted to 1.9×10^4 cells per well. 190 µl cell suspension was added to the assay plates prepared in previous step. Row A containing cell suspension was set aside for no-growth control (day 0). The plates were incubated at 37°C in a humidified incubator with 5% CO_2 for 24 hr. The cell monolayers were fixed with 100 µl of cold 10% w/v trichloroacetic acid by adding it to each well and incubated at 4°C for 1 hr and dried. The cell monolayers were then stained with 100 µl of 0.057% w/v SRB solution.

Unbound dye was removed by repeated washing with 1% v/v acetic acid, and dried. Protein bound dye was extracted with 200 µl of 10 mM unbuffered Trisbase (Tris hydroxyl methyl aminomethane) solution from stained cells. The optical density (OD) was measured using micro plate reader (Bio-rad, ELISA plate reader) at a wavelength of 540 nm. The percentage of cell growth inhibition was calculated by following equation:

$$\%\ \text{Control of cell growth} = 100 - \left(\frac{\text{Mean OD of individual test group}}{\text{mean OD of control group}} \right) \times 100$$

The results were reported in terms of GI_{50} (50% cell-growth inhibition).

6.1.1.13 *In-vivo* anticancer activity

In-vivo anticancer activity was evaluated using murine colon-26 tumor-bearing BALB/c mice (either sex, 6-8 weeks old and ~ 18-22 g body weight). The mice were fed with regular diet and allowed free access to double-distilled water. Twenty four mice were inoculated with colon-26 CRC cells in the dorsal right hind limb area (1×10^7 cells/mice) (Morton *et al.,* 2007). Fifth day after colon-26 cells inoculation, the mice with carcinomas of ~ 8 mm^3 in diameter were divided into four groups of six mice each. Group I kept as control while group II, II and IV were fed with pure CUR, PM and optimized C-LPNCs, respectively. The dose of CUR was same in all the groups i.e. equivalent to 50 mg/kg. All the formulations were administered orally to mice every day for 30 days continuously. The control group received same repetitive oral administration of saline solution. The volumes of solid tumor were measured with a digital max-cal caliper daily and were calculated according to the equation:

$$V\ (mm^3) = [\{(d_1+d_2)/2\}^3] \times 0.5236$$

Where, $[(d_1+d_2)/2]$ = d; the average diameter which is raised to the power 3 i.e. d × d × d; this is then multiplied by the factor (Pi/6) which is equal to 0.5236. Further, Survival of the animals was also monitored for 30 days.

6.1.1.14 Statistical analysis

All the experiments were performed in triplicate and the results were expressed as mean±standard deviation (SD) for *in-vitro* studies and mean±standard errors mean (SEM) for *in-vivo* studies. The statistical analysis was performed with Graphpad Prism Software (version 5.03). Statistical comparisons of the results in reference to control were performed with the analysis of variance (ANOVA).

6.1.2 RESULTS AND DISCUSSION

6.1.2.1 Preparation of C-LPNCs by high speed homogenization method

The Homogenization speed is related to shear rate, which is one strategy to provide high energy input. In the preparation of C-LPNCs require high energy (Garg *et al.,* 2007), reasonable to increase the homogenization speed in order to reduce particle size of C-LPNCs. The homogenization speed accompanied by time is very important factor which dictates the total energy input in the preparation of C-LPNCs. At relatively higher shear rate, C-LPNCs would be broken down to non-equilibrium dispersed structures which are more likely to agglomerate into unstable larger particles (Barauskas *et al.,* 2005). The medium value of duration appears to be advantageous because prolonged duration lead to C-LPNCs destruction and lower duration value lead to failure in C-LPNCs formation. With respect to temperature, a high value supplies more energy during the process and thus favors not only the formation of C-LPNCs but also the reduction in particle size (Garg *et al.,* 2007). This is because appropriate heat provided in the C-LPNCs preparation will lead to uniformity of size, homogeneity of shape and stability after the production phase (Barauskas *et al.,* 2005).

6.1.2.2 Characterization studies

6.1.2.2.1 Mean particle size, polydispersity index and zeta potential

PS, PDI and ZP of different prepared batches are shown in Table 6.3. The PS of the prepared C-LPNCs was found to be in the range of 108±3.4 to 456±7.3

nm. The results showed that the concentration of stabilizing agent (PLX188) and homogenization speed (rpm) were critical parameters for the PS. The PS was found to decrease with increase in the PLX188 concentration (i.e. inversely proportional). This could be attributed to the semi crystalline nature of PLX188 which strongly adsorb onto the surface of C-LPNCs via their hydrophobic POP center block and POE chains (Lee *et al.,* 2008). A higher PLX188 concentration reduces the interfacial tension and facilitates partitioning during homogenization (Kheradmandnia *et al.,* 2010). The PDI values of different batches were found to be in the range of 0.167±0.02 to 0.816±0.03. The small value of PDI (<0.20) indicates a homogeneous C-LPNCs, whereas a larger PDI (>0.3) value indicates heterogeneity (Oliveira *et al.,* 2013). Further, C-LPNCs exhibited negative zeta potential values in the range of -20.4±0.91 to -28.5±0.67 mV, which is attributed to the hydroxyl groups of maltodextrin of SMD that are deprotonated in their ionized form near neutral pH values (Christopher *et al.,* 1999). Large absolute values of ZP indicate the presence of a high electric charge on the C-LPNCs surface. The negative ZP helps the C-LPNCs to repel each other and ensure long term stability followed by avoidance of aggregation (Yousefi *et al.,* 2009).

6.1.2.2.2 Entrapment efficiency and drug loading

Table 6.3 shows %EE and %DL of the prepared C-LPNCs formulation. The aqueous PLX188 solution was used as an external phase to avoid CUR degradation during encapsulation process. The %EE values were found to be in the range of 62.11±0.89% to 88.75±0.2% while the %DL varied from 0.149±0.07% to 0.438±0.09%, which was attributed to better affinity of drug for maltodextrin. At higher level of maltodextrin concentration in SMD, the viscosity of maltodextrin phase increases which ultimately decrease the net shear stress during emulsification and formed larger droplets. Also, the decreased drug diffusion into external aqueous phase due to less shear stress resulted in more entrapment of CUR into the core of maltodextrin (Singh *et al.,* 2010).

Table 6.3 Physicochemical parameters; PS, ZP, PDI, %EE and %DL of various batches (All values reported are mean±SD; n = 3)

Batches	PS(nm)	ZP(mV)	PDI	%EE	%DL
C-SMD1	346±1.5	-23.6±1.67	0.389±0.04	81.22±0.7	0.317±0.02
C-SMD2	263±1.8	-24.8±1.39	0.342±0.06	73.42±0.4	0.212±0.05
C-SMD3	108±3.4	-20.4±0.91	0.167±0.02	65.29±1.0	0.149±0.07
C-SMD4	232±4.6	-21.6±1.10	0.218±0.05	88.75±0.2	0.405±0.01
C-SMD5	189±2.7	-25.3±0.98	0.734±0.07	78.15±0.9	0.276±0.03
C-SMD6	456±7.3	-24.6±1.04	0.471±0.08	68.26±0.7	0.284±0.08
C-SMD7	113±6.2	-28.5±0.67	0.301±0.03	62.11±0.89	0.313±0.06
C-SMD8	125±4.9	-25.9±1.98	0.289±0.06	72.22±0.5	0.438±0.09
C-SMD9	427±2.6	-22.3±1.27	0.816±0.03	67.19±0.3	0.312±0.04

Where; PS: mean particle size; ZP: zeta potential; PDI: polydispersity index; %EE: percent entrapment efficiency; %DL: percent drug loading

6.1.2.3 Design of experiment and statistical analysis

6.1.2.3.1 Formulation optimization using TOED

TOED is one way to qualitatively analyze the correlations between relevant variables at different levels (Chaurasia *et al.,* 2014). Based on the different formulations and process parameters, an orthogonal experimental design using four factors and three levels was performed to optimize the C-LPNCs. The dependent variables considered were PS and %EE. Thus, the PS_i, $\%EE_i$ and delta values were calculated for each response. The factors influencing the PS in decreasing order were as C>D>B>A according to the delta value. In addition, the influence on the PS at individual levels within each factor are explained by PS_i values and can be ranked as: A: 3>1>2; B: 2>1>3; C: 3>2>1; D: 3>2>1 are shown in Table 6.4 and Figure 6.2, respectively. Based on PS_i and delta values, the optimized formulation was found to be $A_3B_2C_3D_3$. Similarly, the sequence of factors influencing the %EE was in order of B>A>C>D based on the delta value and the individual levels within each factor are ranked as: A: 1>3>2;

B: 3>2>1; C: 1>3>2; D: 2>3>1 are shown in Table 6.4 and Figure 6.2, respectively. The $A_1B_3C_1D_2$ was found to be optimized formulation having highest %EE. The different levels of optimized batch for PS and %EE signify that both the responses do not have their desired values at the same variable setting. ANOVA results along with delta value suggested that factors C and D were highly significant in determining PS with a *p* value of 0.021 and 0.004, respectively at 95% confidence level. Thus, other two factors have arbitrary effect on the response. Factors A and B, with *p* values of 0.014 and 0.009, respectively, were found to have significant effects on %EE are shown in Table 6.5. Therefore, the level settings C_3D_3 and A_1B_3 were having significant importance on the PS and %EE, respectively. Based on the levels decided by mean values and ANOVA, the C-LPNCs (batch C-SMD3) was considered to be optimized batch having independent variables as 5 mg CUR, 0.9% w/v SMD, 2.0% w/v PLX188 and 14000 rpm homogenization speed.

Table 6.4 Experimental mean value for the response parameters at different levels of the prepared C-LPNCs according to TOED

Levels	**Independent Factors**			
	A	**B**	**C**	**D**
PS_1	120.62	117.22	156.78	161.47
PS_2	148.60	97.73	155.17	141.22
PS_3	113.12	167.38	70.38	79.65
Delta value	35.48	69.65	86.40	81.82
Rank	4	3	1	2
EE_1	37.01	42.31	37.27	38.08
EE_2	39.49	37.60	38.38	37.63
EE_3	37.20	33.79	38.06	37.99
Delta value	2.49	8.52	1.11	0.45
Rank	2	1	3	4

PS_i and EE_i is the mean value of PS and EE.
Delta value is the difference between the maximum value and the minimum value of PS_i and EE_i.

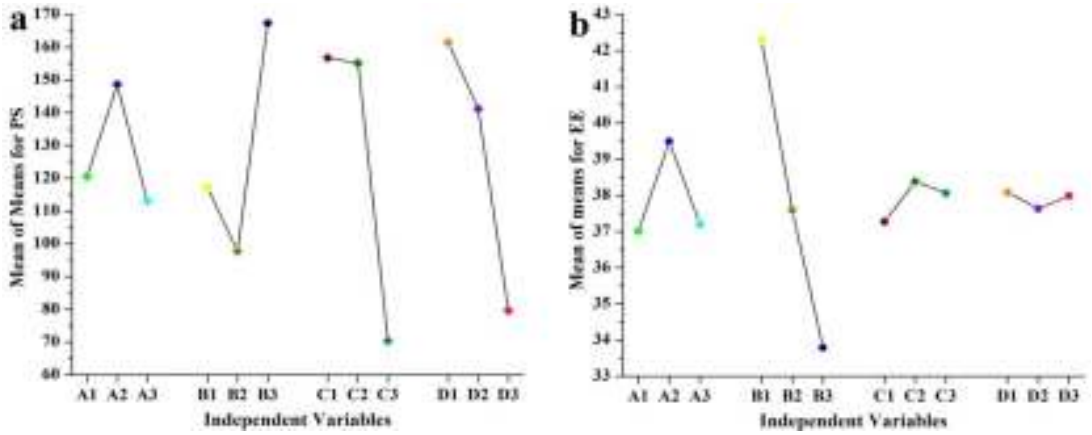

Figure 6.2 Marginal mean graphs of the mean for (a) PS and (b) EE

Table 6.5 ANOVA table for the response parameters of PS and EE

Factors	DoF	SS	MS	%PC	F[a]	P[b]
PS						
A	(2)	(2098.4)	(1049.19)	5.9283	pooled	
B	(2)	(7747.4)	(3873.71)	21.8878	pooled	
C	2	14655.8	7327.89	41.4051	2.977	0.021
D	2	10894.5	5447.24	30.7788	2.213	0.004
Pooled Error	(4)	(9845.8)	(4922.9)			
SS_{Total}	8	35396.1		100		
%EE						
A	2	11.482	5.7411	9.3261	0.186	0.014
B	2	109.338	54.6689	88.8082	1.776	0.009
C	(2)	(1.959)	(0.9793)	1.5911	pooled	
D	(2)	(0.338)	(0.1692)	0.2745	pooled	
Pooled Error	(4)	(2.297)	(61.5585)			
SS_{Total}	8	123.117		100		

DoF; degree of freedom, SS; sum of squares, MS; mean of squares, %PC; percent contribution, F; fisher test

[a] $F_{0.05}$ *(2,4)=6.94*

[b] *P<0.05; significant in C and D for PS and in A and B for %EE.*

6.1.2.4 Solid state characterization

6.1.2.4.1 Fourier transform infrared spectroscopy study

The FTIR spectra for pure CUR, SMD, PM and optimized C-LPNCs (batch C-SMD3), are shown in Figure 6.3. The FTIR spectrum of pure CUR (Figure 6.3a) shows characteristics absorption peaks at 3,489 cm^{-1} which represent phenolic -OH stretching vibration, at 1,629 cm^{-1} the C=O stretching peak of conjugated ketone, sharp absorption peaks at 1,600 cm^{-1} represent stretching vibrations of benzene ring and at 1,371-1,390 cm^{-1} the stretching and deformation of methyl groups (Pan *et al.,* 2007). FTIR spectra of maltodextrin in SMD (Figure 6.3b) shows the strong broad band between 972 cm^{-1} and 1,201 cm^{-1} represents most characteristic peaks of the maltodextrin. This attributed to C-O stretching vibrations. In addition, at 1,240 cm^{-1} represents the presence of P=O (phosphomoyl) group and peak at 1,145 cm^{-1} represents the presence of P-O-C vibrations due to the presence of phosphatidylcholine in SMD. Therefore, All major peaks of CUR and SMD were observed in FTIR spectra of PM, as illustrated in Figure 6.3c. In optimized C-LPNCs a shift from 3,489 cm^{-1} to 3,392 cm^{-1} is shown in Figure 6.3d and the peak at 3,392 cm^{-1} becomes wider, which indicates hydrogen bonding is enhanced (Pan *et al.,* 2007). All of the above indicating bands were observed in optimized C-LPNCs without changing their positions. These results clearly indicate the CUR present in dispersed conditions in LPNCs and no any specific interaction was observed in PM and optimized C-LPNCs.

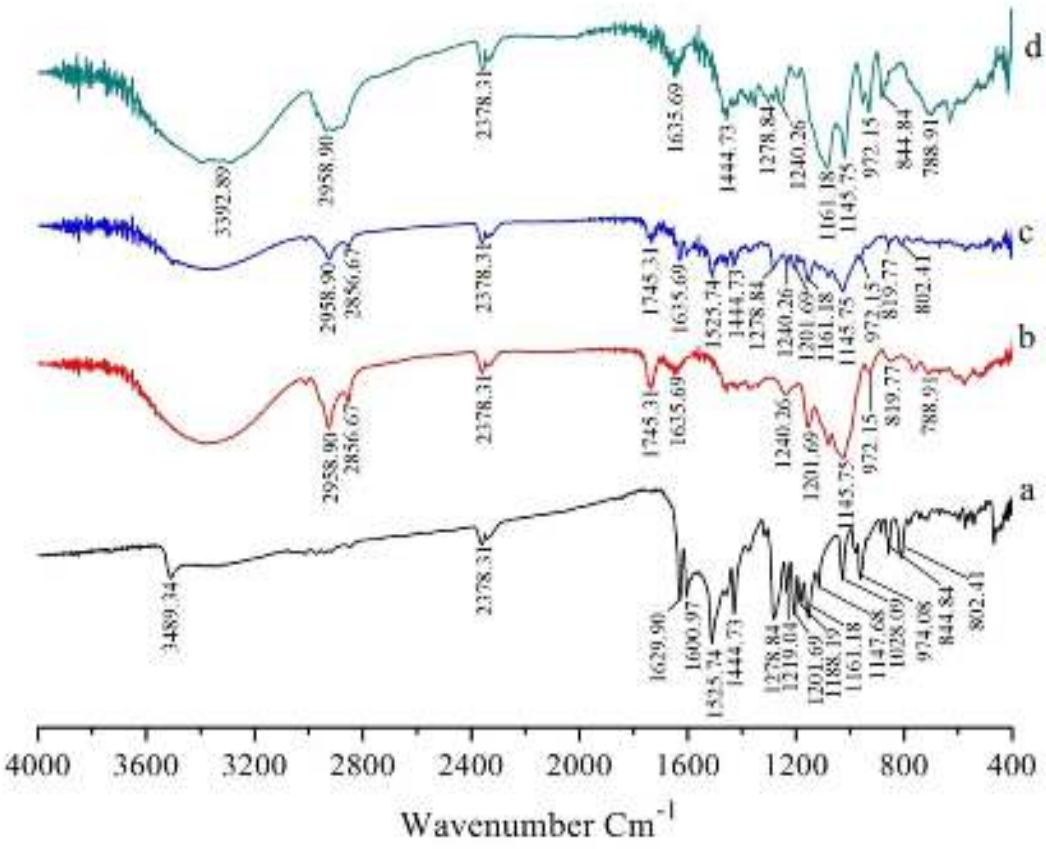

Figure 6.3 FTIR spectra of (a) pure CUR (b) SMD (c) PM and (d) optimized C-LPNCs.

6.1.2.4.2 Differential scanning calorimetric study

DSC thermograms of pure CUR, SMD, PM and optimized C-LPNCs are shown in Figure 6.4. Both pure CUR and PM exhibited a melting temperature of the drug followed by a sharp endothermic decomposition peak at 180°C as illustrated in Figure 6.4a and 6.4c, respectively. In SMD thermograms no distinct melting temperature was observed, which clearly indicated that SMD was thermally stable upto 250°C as shown in Figure 6.4b. The DSC thermograms did not detect any crystalline drug material in optimized C-LPNCs as the sharp peak of CUR was absent as illustrated in Figure 6.4d. Thus, it seemed that the CUR was encapsulated into the core of maltodextrin as amorphous matrices (Acharya *et al.,* 2009).

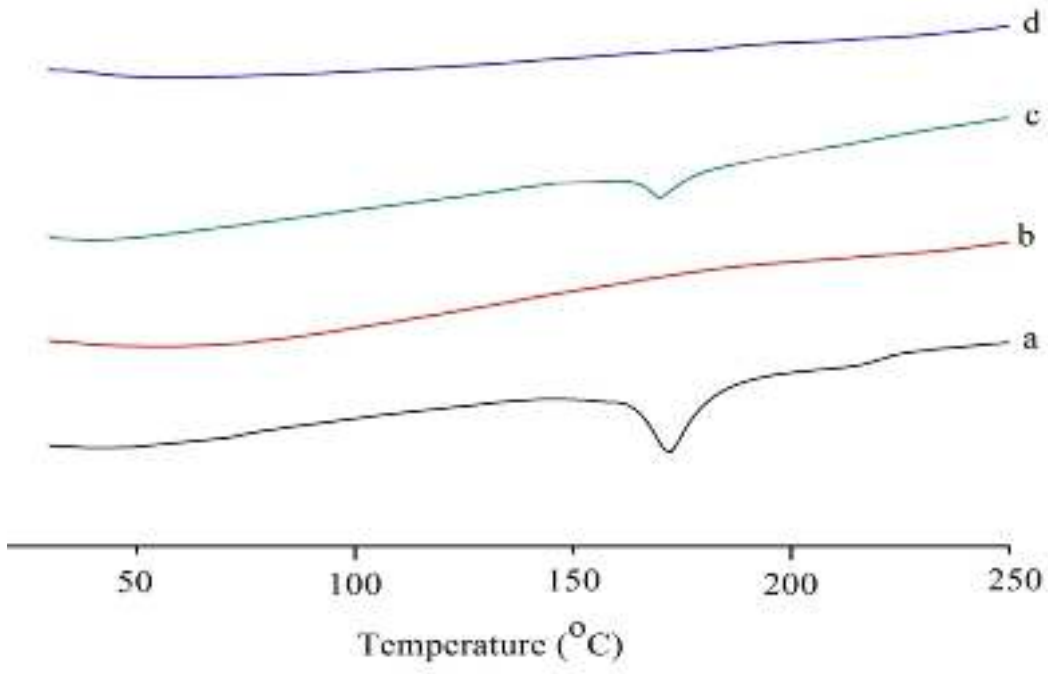

Figure 6.4 DSC thermograms of (a) pure CUR (b) SMD (c) PM and (d) optimized C-LPNCs.

6.1.2.4.3 Powder X-ray diffraction study

X-ray diffractogarms of pure CUR, SMD, PM and optimized C-LPNCs are shown in Figure 6.5. Pure CUR and SMD showed several characteristic peaks at 2θ angles as shown in Figure 6.5a and 6.5b, respectively, which demonstrates the traits of high crystalline structure. In case of PM, although most of the peaks were disappeared, peaks at 17.5°, 22.5°, and 31.0° were still observed as illustrated in Figure 6.5c. Since SMD provided no characteristic peaks, these three peaks must originate from crystalline form of CUR which indicated that CUR was partially present in crystalline form in the PM followed by partial transformation into amorphous form. However, there was absence of all characteristics CUR peaks when entrapped in LPNCs as illustrated in Figure 6.5d. This absence of detectable crystalline domains of CUR in optimized C-LPNCs clearly indicates that CUR encapsulated in maltodextrin of SMD as an amorphous form or disordered-crystalline phase which leads to easy diffusion of drug molecule followed by sustained release of the encapsulated CUR (Kumar *et al.,* 2014).

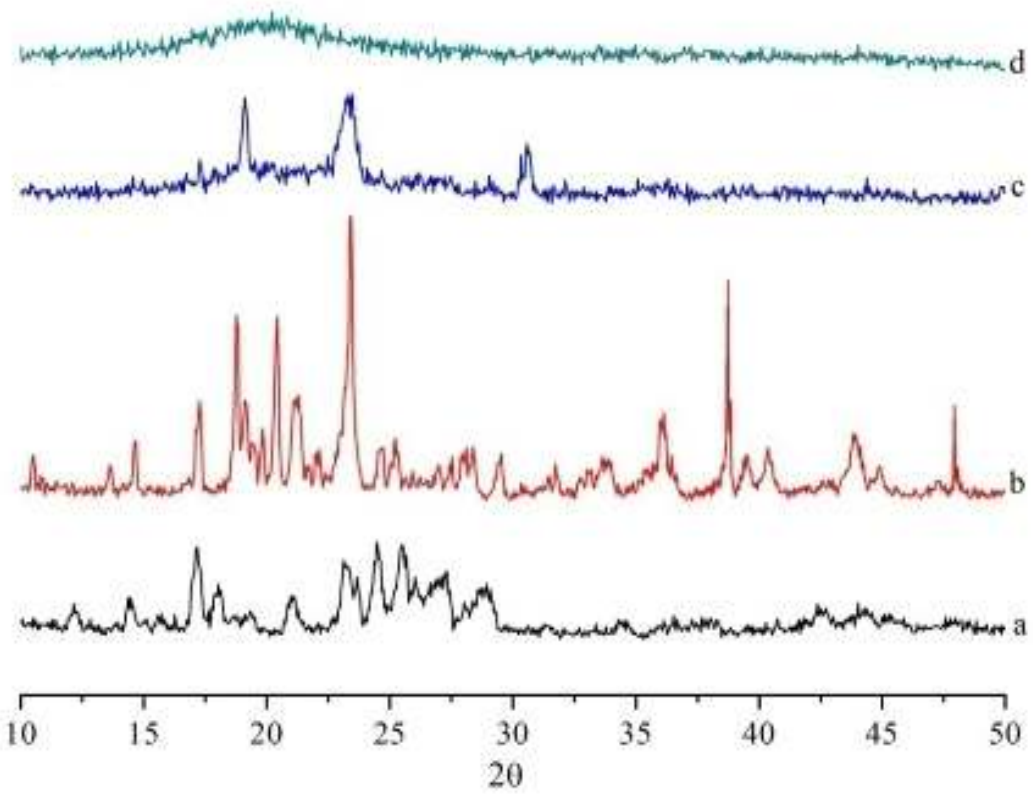

Figure 6.5 *p*XRD curves of (a) pure CUR (b) SMD (c) PM and (d) optimized C-LPNCs.

6.1.2.5 Morphological evaluation

6.1.2.5.1 High resolution transmission electron microscopy study

HR-TEM study was performed in order to examine the surface morphology of the optimized C-LPNCs. The TEM micrographs exhibited well separated spherical C-LPNCs having smooth surface as shown in Figure 6.6a. The micrographs also revealed that the C-LPNCs have almost uniform size distribution with low polydispersity and most of them are smaller than 115 nm. Further, the crystallinity of the drug was also studied with electron diffraction (ED) pattern. The absence of star shaped particles in the ring patterns and presence of an amorphous diffraction halo in the ED (Figure 6.6b) confirms the amorphous and homogeneous distribution of drug into the LPNCs which also correlated very well with the results of DSC and XRD study (Chaurasia *et al.,* 2014).

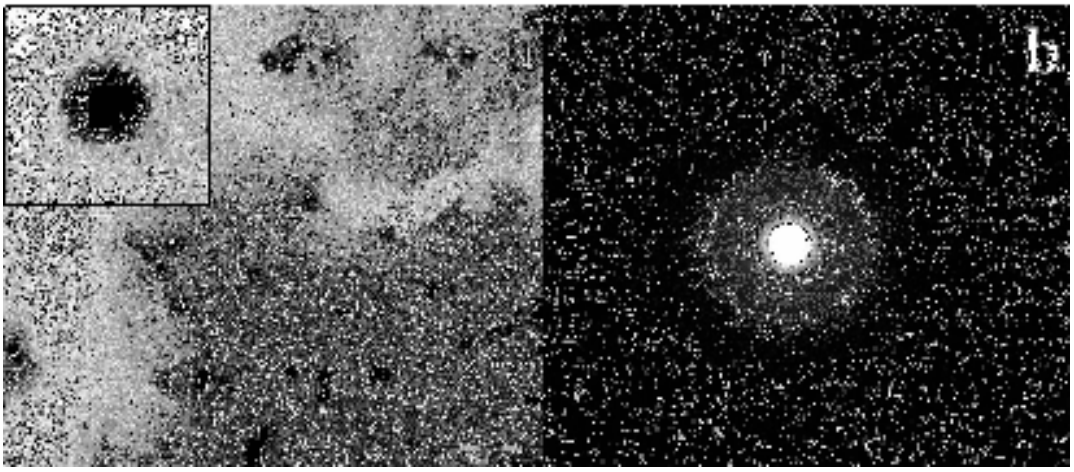

Figure 6.6 (a) HR-TEM micrographs at ×20,000 magnification (bar=500nm) and (b) electron diffraction pattern of optimized C-LPNCs.

6.1.2.5.2 Atomic force microscopy study

AFM has employed as a new tool for surface morphology of C-LPNCs. In this technique, the force, acting between a surface and probing tip resulting in a spatial resolution up to 0.01 nm, are used for the imaging of the surface of C-LPNCs. The preparation of sample is very simple in this technique as vacuum or conductivity of sample is not mandatory. Therefore, direct analysis of originally hydrated or solvent containing samples is possible by this technique. The AFM micrographs of prepared C-LPNCs exhibited well separated spherical shape nanoparticles with smooth surfaces as shown in Figure 6.7. The micrographs also revealed that the C-LPNCs have an almost uniform size distribution with low polydispersity and most of them have average diameter smaller than 115 nm as measured by particle size analyzer.

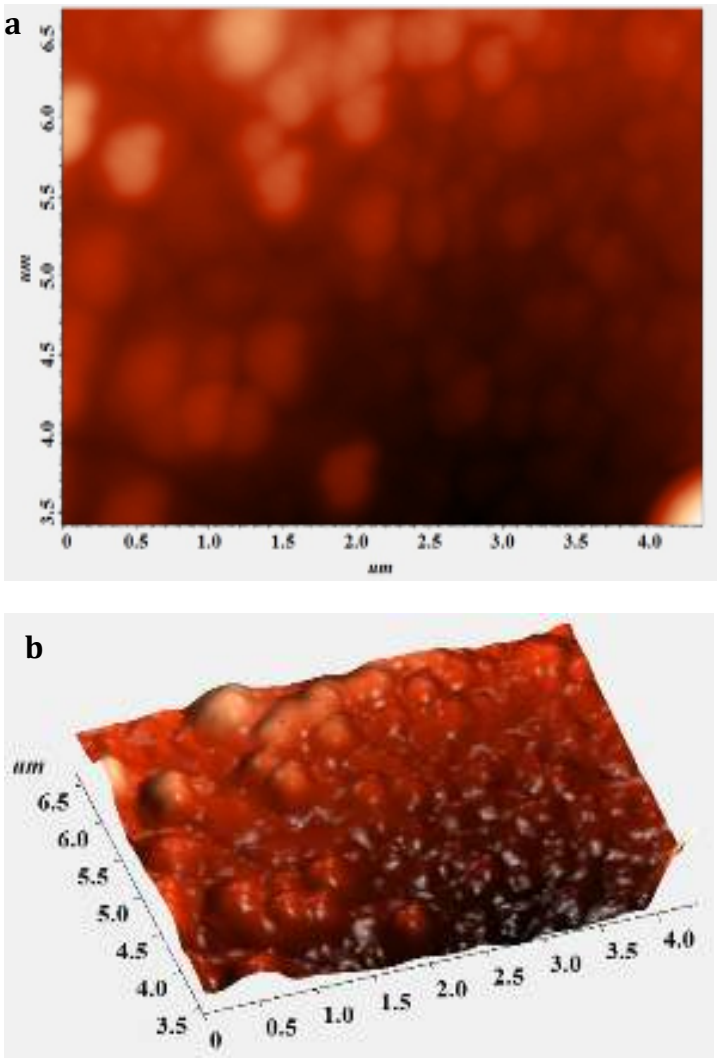

Figure 6.7 AFM micrographs of the optimized C-LPNCs (a) 2D image (b) corresponding 3D image.

6.1.2.6 Evaluation of drug distribution within the LPNCs

The distribution of drug within the LPNCs was confirmed by CLSM micrographs as shown in Figure 6.8. The optimized C-LPNCs appearing green entrapped inside the core of maltodextrin in SMD. The CUR seen to be uniformly distributed within the C-LPNCs (Mukherjee & Viswanatha, 2009). This is a critical parameter that would help in uniform drug release from the C-LPNCs once they will be administered *in-vivo.*

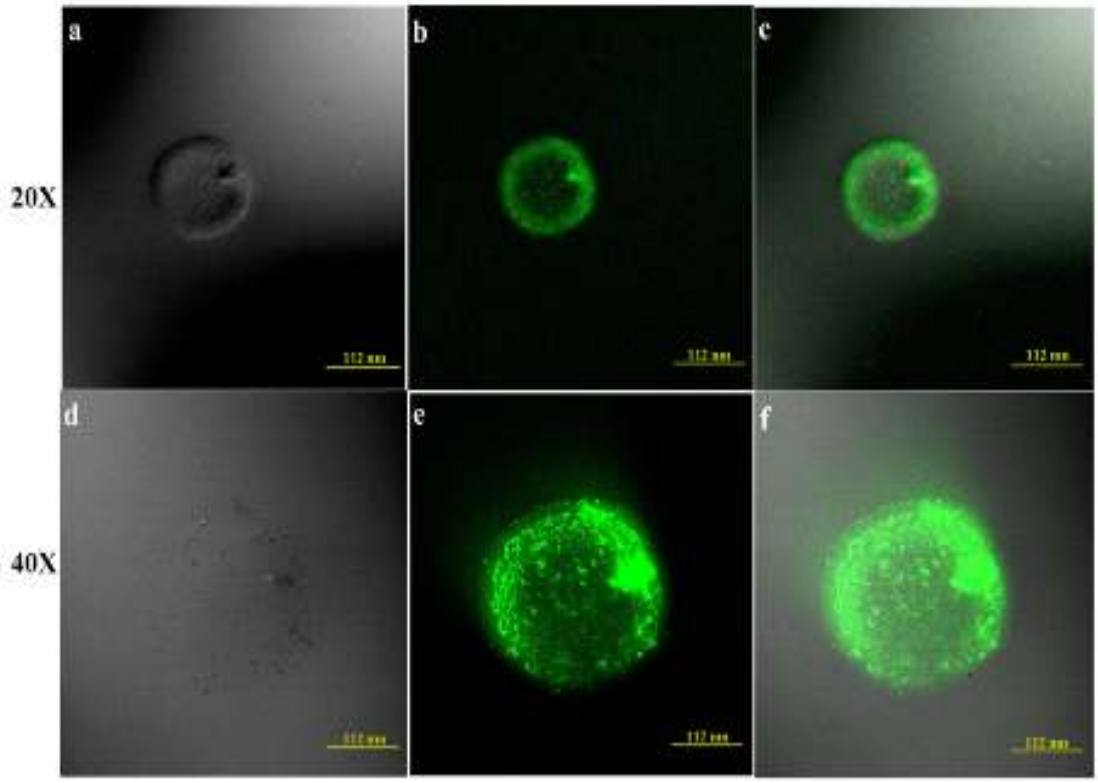

Figure 6.8 CLSM images illustrating the encapsulation and distribution of CUR (green fluorescence) within the C-LPNCs. a and d DIC image, b and e fluorescent image, c and f merged of fluorescent and DIC image at magnification 20X and 40X, respectively.

6.1.2.7 Analysis of photophysical properties

To confirm the entrapment of CUR into the core of C-LPNCs, the photophysical property of CUR was taken into consideration. Pure CUR in PBS, pH 7.4 solution showed a distinct high absorbance peak at around 420 nm. The absorbance intensity of C-LPNCs showed less intense peak at the same wavelength of pure CUR as illustrated in Figure 6.9. This result confirms that successful incorporation of CUR into the water soluble hosts such as SMD in the form of C-LPNCs, will increase hydrolytic stability and resistance to extensive intestinal and hepatic metabolism (Priyadarsini, 2009).

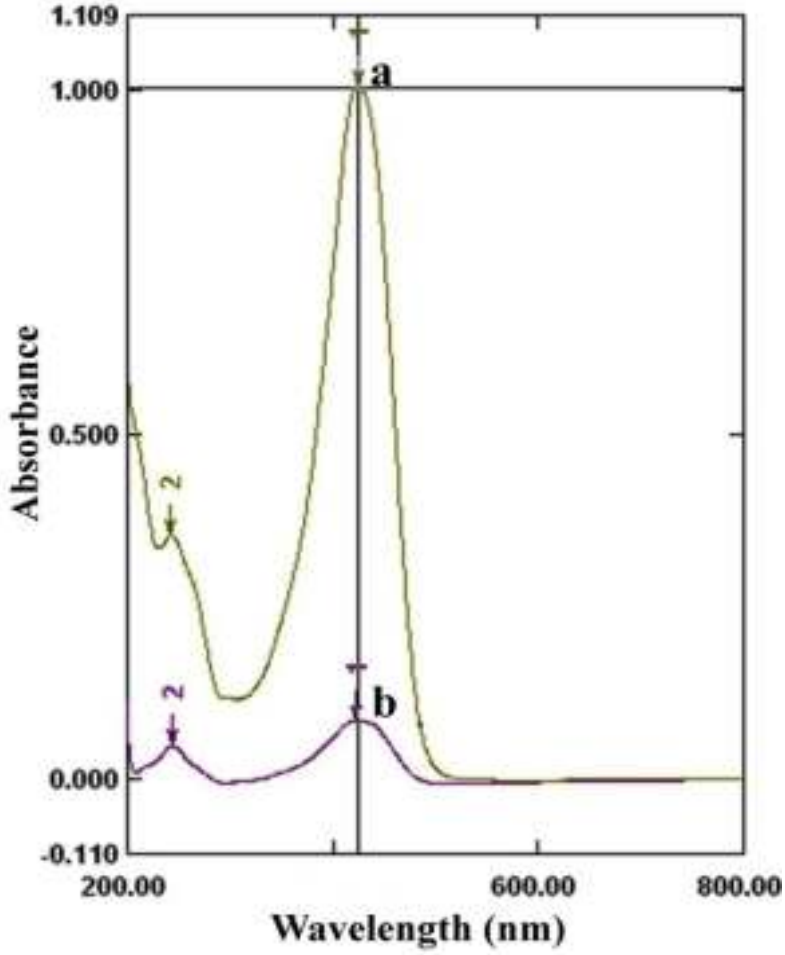

Figure 6.9 Ultraviolet-Visible absorbance spectra of (a) pure CUR and (b) optimized C-LPNCs in PBS, pH 7.4.

6.1.2.8 *In-vitro* drug release and kinetic profile

Figure 6.10 illustrates the *in-vitro* release profiles of pure CUR and optimized C-LPNCs in PBS, pH 7.4 before and after 3 months of storage. The pure CUR is practically insoluble in PBS, pH 7.4 as compared to optimized C-LPNCs. The optimized C-LPNCs gave >80% drug release at the end of 24 hr. The enhanced drug release was due to the structural homogeneity and amorphous nature of the CUR in LPNCs which facilitate higher solubility (Adibkia *et al.,* 2007). However, they provided a burst release during first 30 min due to a simultaneous release of surface bound drug (being more than 16%) followed by hydration and swelling of the C-LPNCs, which eventually lead to a diffusion-controlled drug release profile lasting up to 24 hr. Hydration brings about an

increment in the diffusional path length of molecules and consequently the rate of CUR diffusion becomes lower (Wong *et al.,* 1999). Therefore, obtaining of controlled release profile and its maintenance could be assumed to be dependent on the relative hydration rate and the integrity of the carrier matrices. These results indicated that the release of CUR from LPNCs was governed by a combination of drug diffusion and fluidization of the carrier matrices.

The rate and extent of drug release might be closely related to the distribution coefficient of the drug. Furthermore, data obtained from *in-vitro* release studies of optimized C-LPNCs were fitted to various kinetic equations such as zero order, first order, Higuchi, Korsmeyer-Peppas models and Hixon-crowel. The Korsmeyer-Peppas model were best fit for CUR release from the C-LPNCs as indicated by a higher correlation coefficient (R^2=0.948) compared with first order (R^2=0.718), Hixon-Crowel (R^2=0.667), zero-order (R^2=0.549) and Higuchi equation (R^2=0.902) as shown in Table 6.6. To further elucidate the release mechanism involved in optimized C-LPNCs, the Korsmeyer-Peppas model was the best fit model with n value 0.462, indicating fickian diffusion mechanism of drug release from the LPNCs (n≤0.5 for fickian diffusion). These results revealed that the optimized C-LPNCs showed a desirable controlled release property and suggested that the drug incorporated into the innermost core of LPNCs was retained for a certain period of time, which released slowly in release media with the function of time.

Table 6.6 Release parameters for optimized C-LPNCs (batch C-SMD3) obtained after fitting *in-vitro* drug release data to five different mathematical models for drug release kinetics

Batch	Zero order	First order	Higuchi model	Hixon-Crowel model	Korsemeyer-Peppas model
C-SMD3	K_z =2.939 (Con./time) R^2=0.549	K_F=0.077 ($Time^{-1}$) R^2=0.718	K_H=18.934 R^2=0.902	K_{HC}=0.084 R^2=0.667	K_p=24.92 R^2=0.948 n=0.462

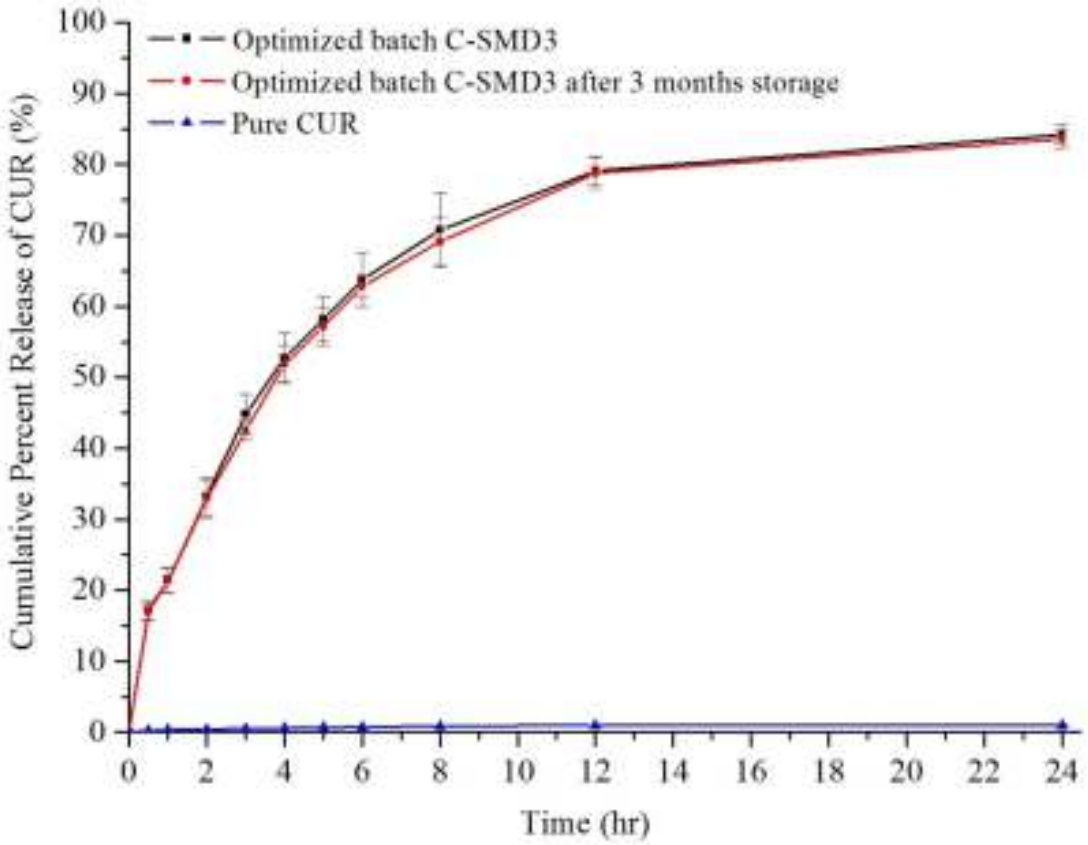

Figure 6.10 *In-vitro* release profile of pure CUR and optimized C-LPNCs (batch C-SMD3) in PBS, pH 7.4 for 24 hr before and after 3 months storage (Vertical bars represent ±SD, n=3).

6.1.2.9 Stability study

The physicochemical parameters of the optimized C-LPNCs were found to be unchanged indicating stability over three months study period. The differences in PS, PDI and %EE were insignificant throughout the stability study indicating that the C-LPNCs were highly stable as depicted in Figure 6.11. The factors contributing to enhanced stability were attributed to protective nature offered by the combinations of the maltodextrin and PLX188 which might have formed an interfacial film as well as a high surface charge that provided droplet-droplet repulsion (Kheradmandnia *et al.,* 2010).

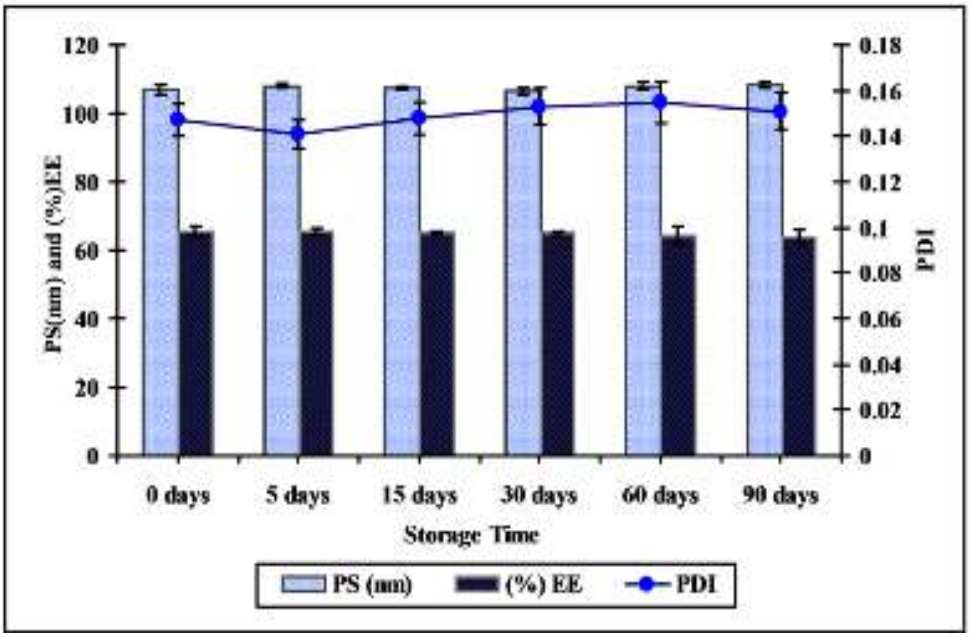

Figure 6.11 Stability data of the optimized C-LPNCs during storage at room temperature (all experiments were performed in triplicate and the vertical bars represent ±SD, n=3).

6.1.2.10 *In-vivo* pharmacokinetic study

The mean plasma concentration-time profiles obtained after oral administration of the pure CUR suspension, PM and optimized C-LPNCs are shown in Figure 6.12. The $AUC_{0\text{-}12}$ and C_{max} value was found to be 38.68-fold, 130.49-fold as well as 55.226-fold, 104.797-fold greater when CUR was administered as PM and optimized C-LPNCs, respectively, compared with pure CUR aqueous suspension as shown in Table 6.7. The plasma levels declined after 2 hr, indicating rapid systemic elimination of pure CUR. This was also evident by short biological half-life i.e. 1.25±0.042 hr for pure CUR. These results indicated that enhanced oral bioavailability of CUR can be observed with PM as well as optimized C-LPNCs; though, the improvement of oral bioavailability in case of optimized C-LPNCs was significantly (p<0.05) much higher than the PM as well as pure CUR. The prevention of degradation of CUR by maltodextrin in GIT might be the possible reasons for improved oral bioavailability of the CUR as CUR was present into the core of maltodextrin. Furthermore, when C-LPNCs absorbed

through specialized M-cells of the payer's patches in the small intestine, they directly drains into the lymphatic system thus prevent the drug from the first pass metabolism in the hepatic tissue (Florence, 1997). Moreover, the maltodextrin as a carrier, might have induced paracellular transport by enhancing intestinal epithelial permeability through opening of the tight junction (Kommuru *et al.,* 2001).

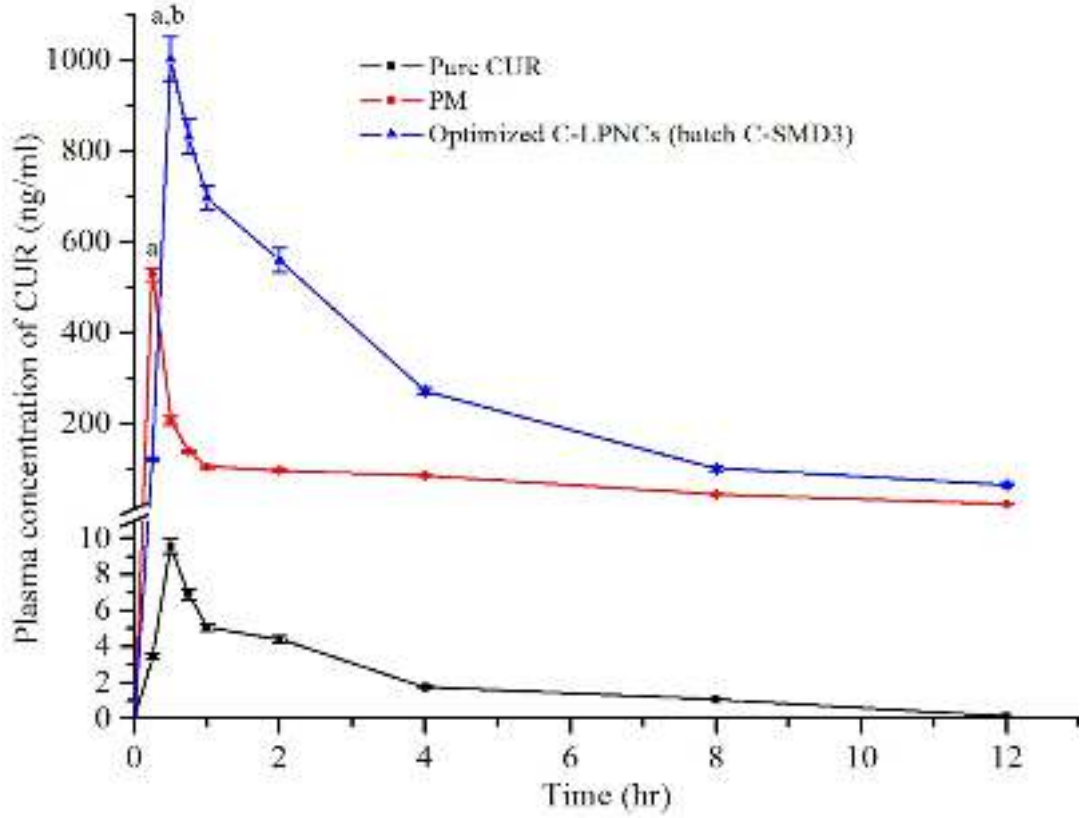

Figure 6.12 Plasma concentrations-time profile after oral administration of pure CUR, PM and Optimized C-LPNCs (dose 50 mg/kg in each case); Vertical bars represent ±SEM; n=6.
[a]*p*<0.05, compared to the control (pure CUR)
[b]*p*<0.05, compared to PM
(One-way ANOVA; Tukey's multiple comparison test).

Table 6.7 Pharmacokinetic parameters after oral administration of PM and optimized C-LPNCs (batch C-SMD3), compared with aqueous suspension of pure CUR (dose 50 mg/kg); All values reported are ±SEM (n=6)

Parameters	Pure CUR (Control)	PM	Optimized C-LPNCs (batch C-SMD3)
C_{max} (ng/ml)	9.582±0.391	529.188±14.729	1004.177±48.553
T_{max} (hr)	0.5±0.0	0.25±0.0	0.5±0.0
AUC_{0-12} (ng/ml).hr	23.225±0.477	898.411±21.218	3030.846±58.141
$AUMC_{0-12}$ (ng/ml).hr^2	74.92±2.031	3571.964±82.199	21070.581±111.439
$t_{1/2}$ (hr)	1.25±0.042	4.273±0.0361	6.907±1.111
MRT (hr)	3.225±0.015	3.975±0.045	6.952±0.679

C_{max}; maximum plasma concentration, T_{max}; time to reach maximum plasma concentration, AUC; area under the plasma concentration-time curve, AUMC; area under the first moment curve, $t_{1/2}$; half life, MRT; mean residence time

6.1.2.11 *In-vitro* cytotoxicity study

The *in-vitro* cytotoxic activity of normal control, pure CUR, PM and optimized C-LPNCs (batch C-SMD3) was evaluated by assessing cell viability using colon-26 cancer cell line. As can be seen in Figure 6.13, a significant (p<0.001) marked reduction in cell viability was observed for all the treatment groups with respect to GI_{50} value. Incubation of cells with 14.423±0.721 µg/ml, 2.381±0.119 µg/ml and 0.636±0.031 µg/ml of pure CUR, PM and optimized C-LPNCs contributed to 50% cell viability, respectively as shown in Table 6.6. Results further indicated that the GI_{50} value of PM and optimized C-LPNCs were found to be ~6-fold and ~23-fold higher, as compared to pure CUR aqueous suspension as illustrated in Figure 6.14. Therefore, it can be concluded that optimized C-LPNCs showed higher cytotoxic action at much lower concentration as compared to PM as well as pure CUR and is indicative of enhanced therapeutic efficacy of CUR. The mechanism involved for enhancement of cytotoxicity activity of C-LPNCs mediated by maltodextrin based lipopolysaccharide, can be explained

by the fact that (a) the host-guest relation of maltodextrin, the LPNCs can adsorb onto the cell membrane leading to increased drug concentration near the cell structure, thus generating a concentration gradient that would favour a drug influx into the cell. (b) Tumor cells (which in many situations exhibited enhanced endocytotic activity) can internalize LPNCs of maltodextrin allowing the drug to be released into the interior of the cells, thus contributing to an increase of the drug concentration near its site of action (Nemati *et al.,* 1994).

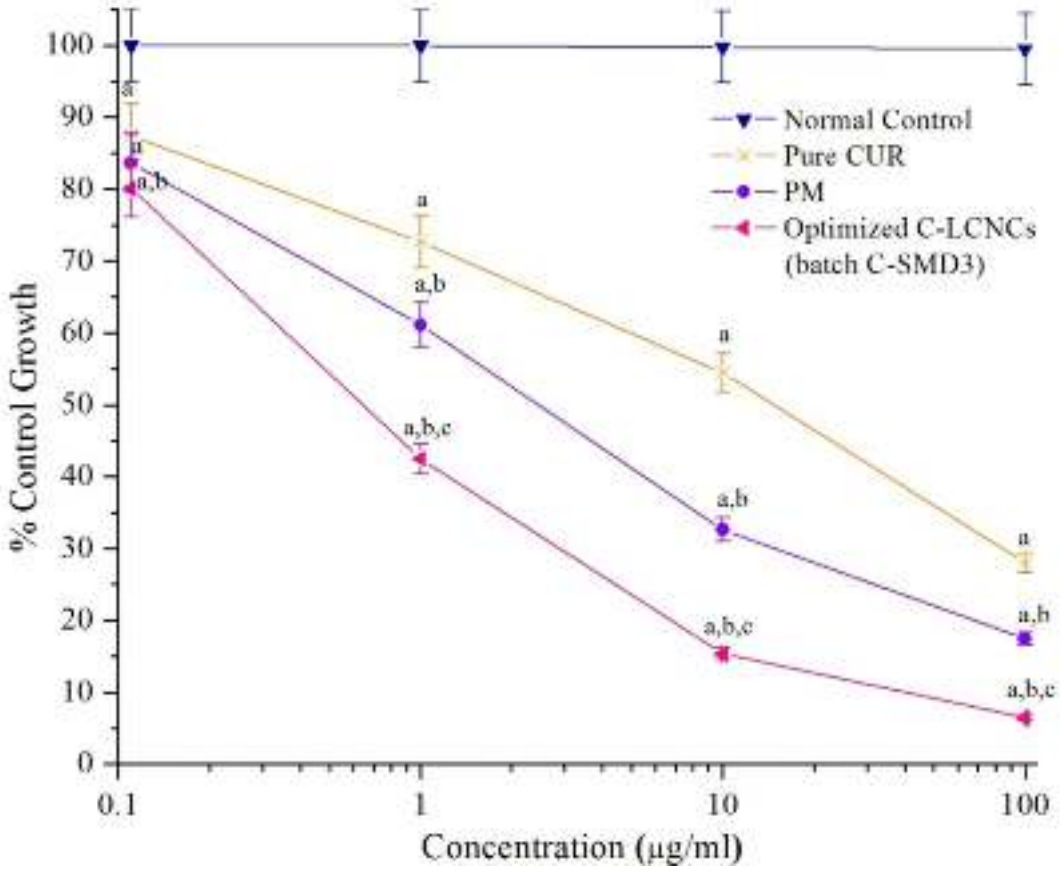

Figure 6.13 *In-vitro* cytotoxicity profile of normal control, pure CUR, PM and optimized C-LPNCs (batch C-SMD3) in colon-26 cancer cell line; Vertical bars represent ±SD; n=3.
[a]*p*<0.001compared to normal control
[b]*p*<0.001 compared to pure CUR
[c]*p*<0.001 compared to PM (Two-way ANOVA; Bonferroni post hoc tests).

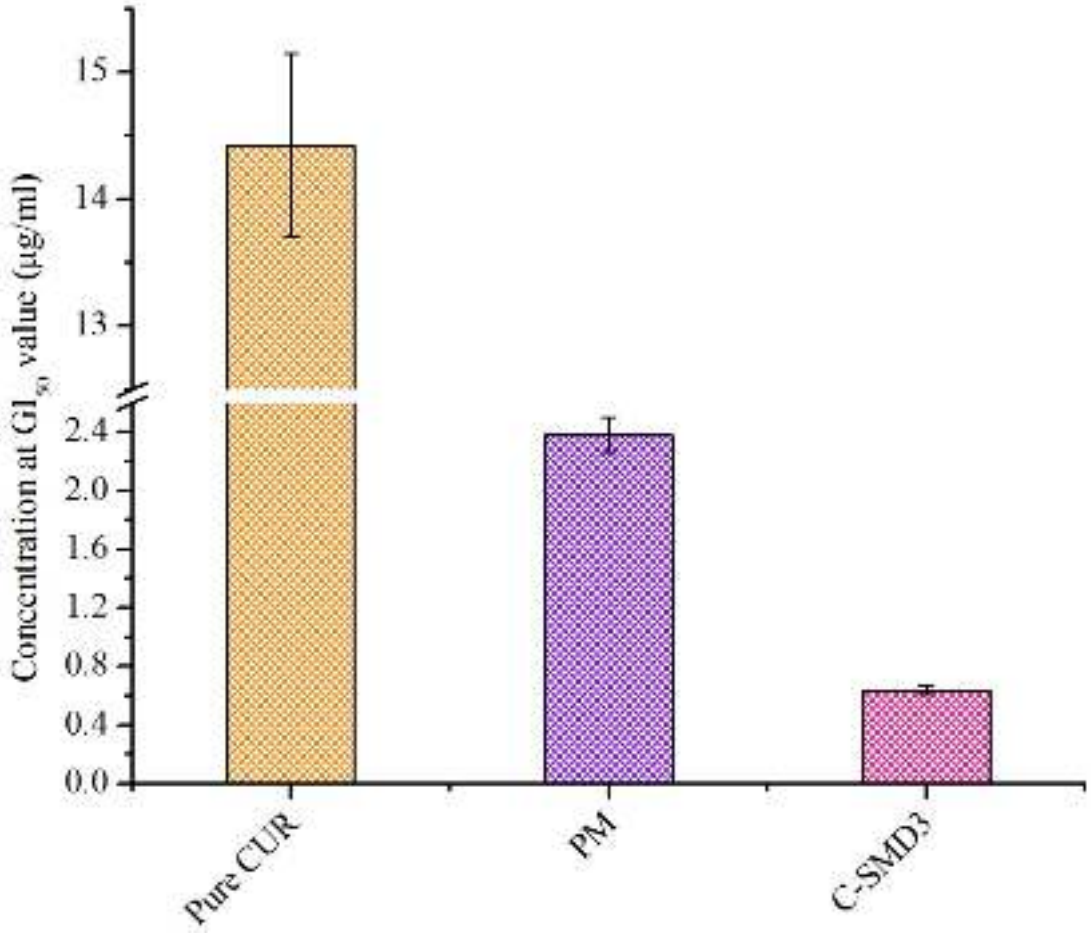

Figure 6.14 The bar chart indicating the concentrations of pure CUR, PM and batch C-SMD3 at GI_{50}; (Vertical bars represent ±SD; n=3).

6.1.1.12 *In-vivo* anticancer activity

Figure 6.15 shows the *in-vivo* anticancer efficacy after repetitive oral administration of pure CUR (50 mg/kg), PM and optimized C-LPNCs (50 mg/kg equivalent to pure CUR) for 30 days. Tumor growth progression clearly indicates that all the formulation significantly inhibited the tumor volume in comparison with control group (p<0.001) (Figure 6.15a). PM resulted into significant tumor growth suppression in comparison to that of pure CUR (p<0.05). However, significantly much higher suppression in the tumor growth was observed in case of optimized C-LPNCs as compared to both PM and pure CUR (p<0.001), respectively (Figure 6.15b).

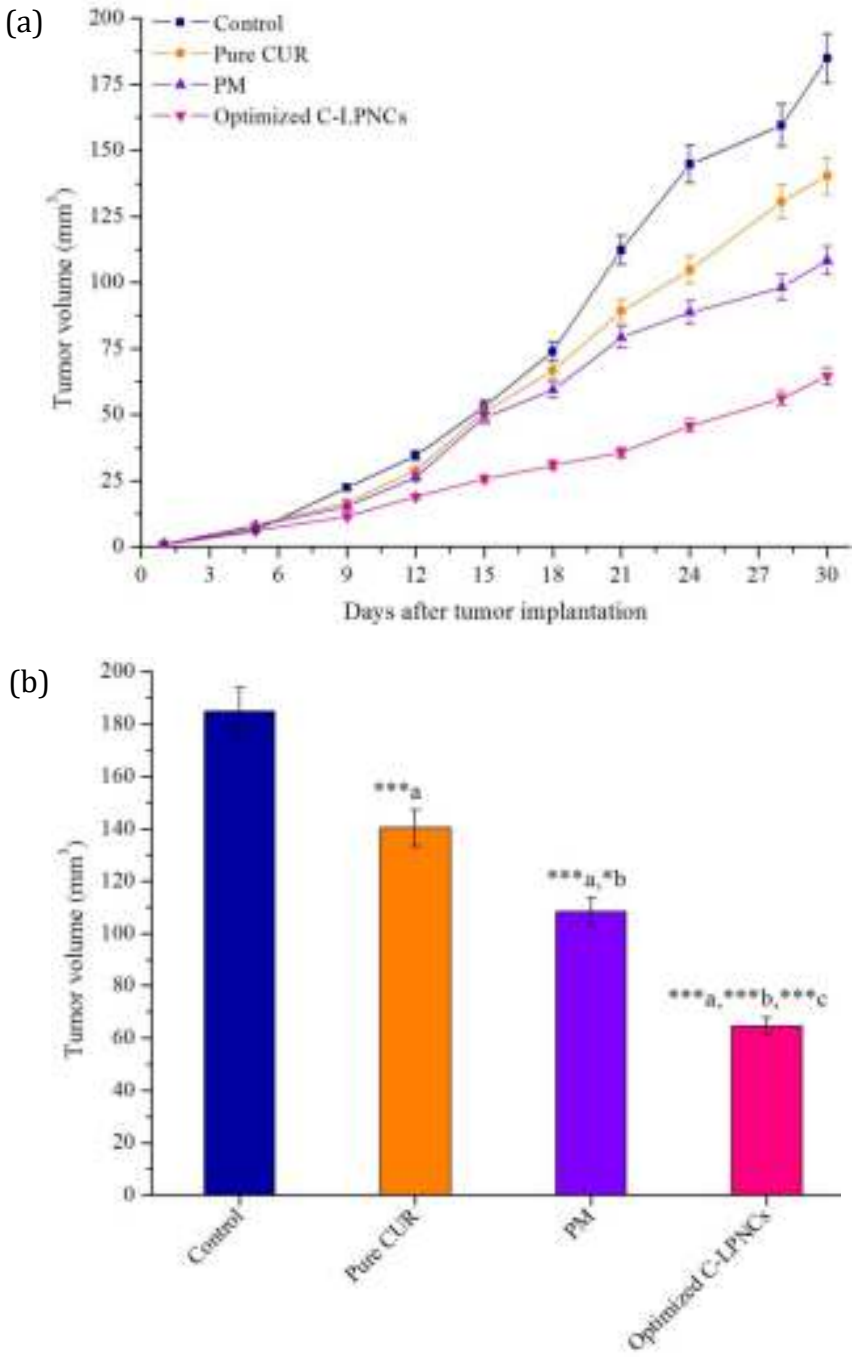

Figure 6.15 (a) Tumor progression curves for tumor-bearing mice which were orally administered with control, pure CUR, PM and optimized C-LPNCs ([CUR]=50 mg/kg) when the tumor volume reached about ~8 mm³ (5th day after inoculating with colon-26 cells to mice). (b) Bar diagram of data from day 30 onwards from "a" part of Figure 6.15;
Vertical bars represent ±SEM; n=6.
(*p<0.001, *p<0.05; a vs control, b vs pure CUR and c vs PM; One-way ANOVA followed by Tukey's multiple comparison test).**

Safety profile of CUR formulations were evaluated by measuring the changes in body weight as a function of time as shown in Figure 6.16. The decrease in body weight was observed in control treated group of mice. The Pure CUR and PM treated group of tumor-bearing mice showed slight increase in body weight. Whereas, optimized C-LPNCs treated group of mice exhibited much increase in body weight as compared to both pure CUR and PM treated groups.

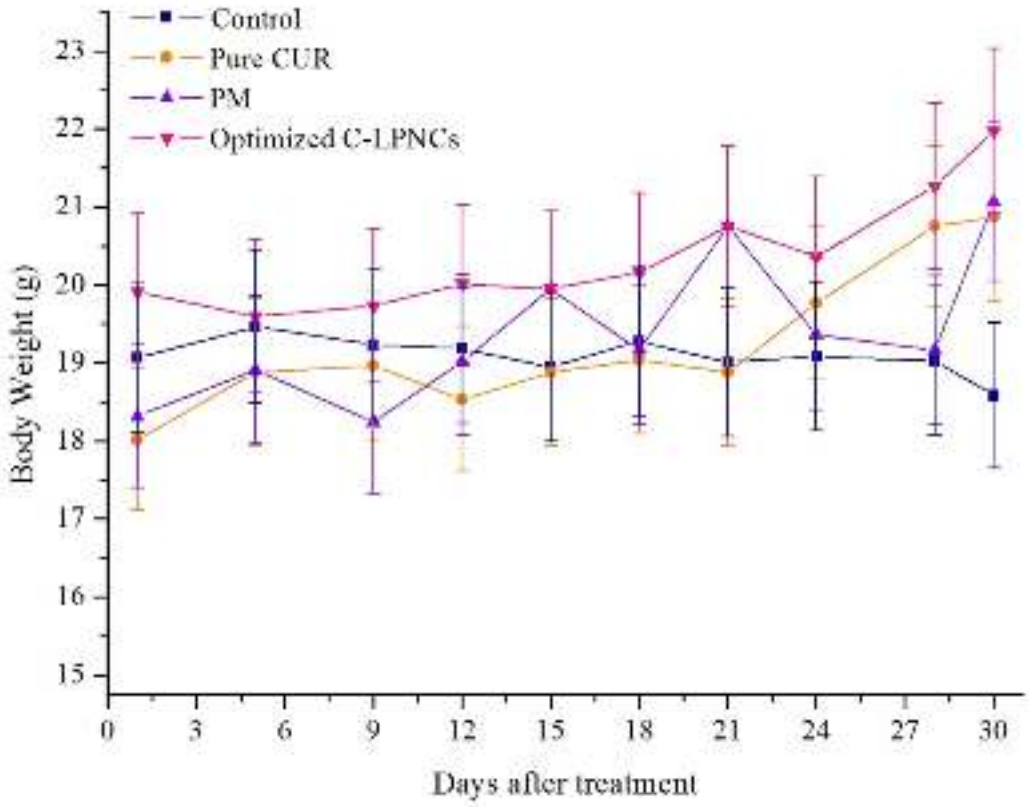

Figure 6.16 Alteration in body weight after incubation of colon-26 cells to mice and treatment with CUR formulations; (Vertical bars represent ±SEM; n=6).

The representative photographs of tumor-bearing mice from control and treatment groups at experimental end point are shown in Figure 6.17.

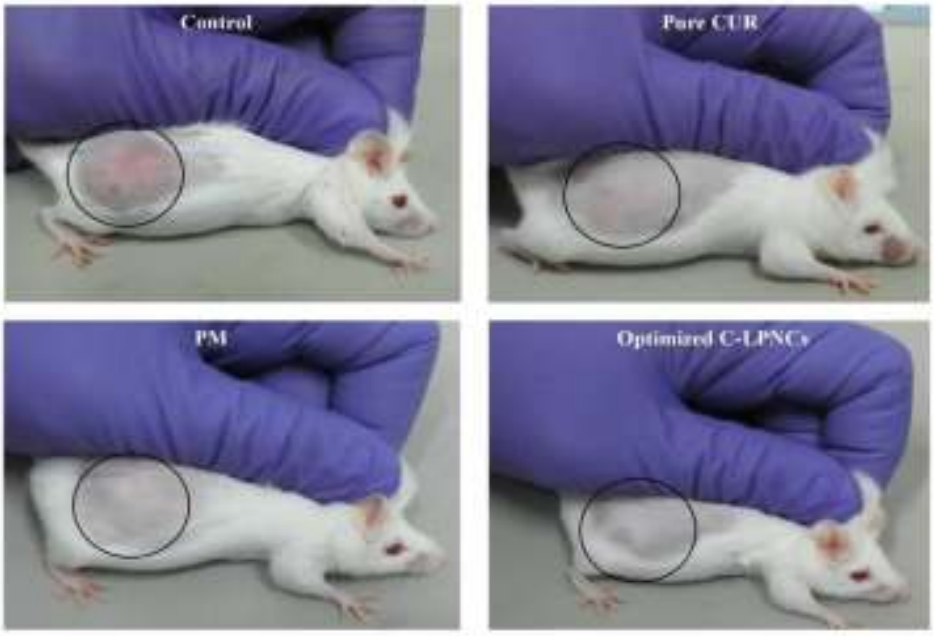

Figure 6.17 Photographs of representative tumor-bearing mice belonging to control and treatment groups at the end of 30 days of inoculation with colon-26 cells. Tumors were indicated within black circles.

Kaplan-Mirer survival plots of animals after 30 days repetitive treatment with control and different CUR formulations as depicted in Figure 6.18. The 100% survival throughout the study period was recorded in the optimized C-LPNCs treated group. Whereas, control treated group of animal showed 16.67% survival. Furthermore, 33.33% survival was observed in the animal groups treated with PM as well as pure CUR.

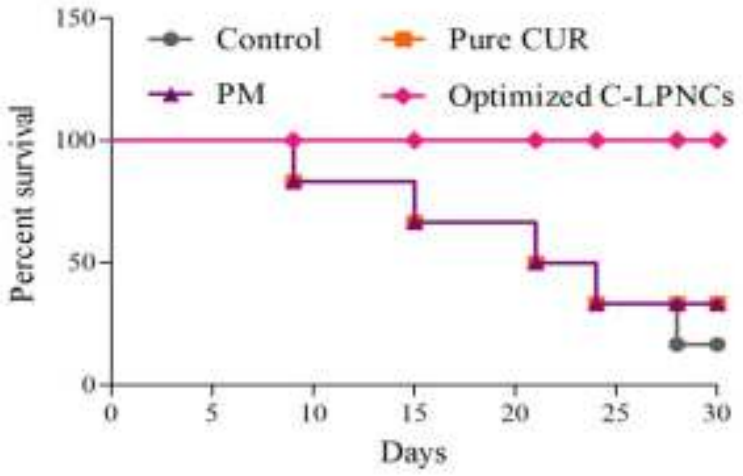

Figure 6.18 Kaplan-Meier survival curve of tumor-bearing mice treated with control and various CUR formulations.

At the end of the treatment, tumors were excised and weighed. The tumor weight of different treatment groups are shown in Figure 6.19.

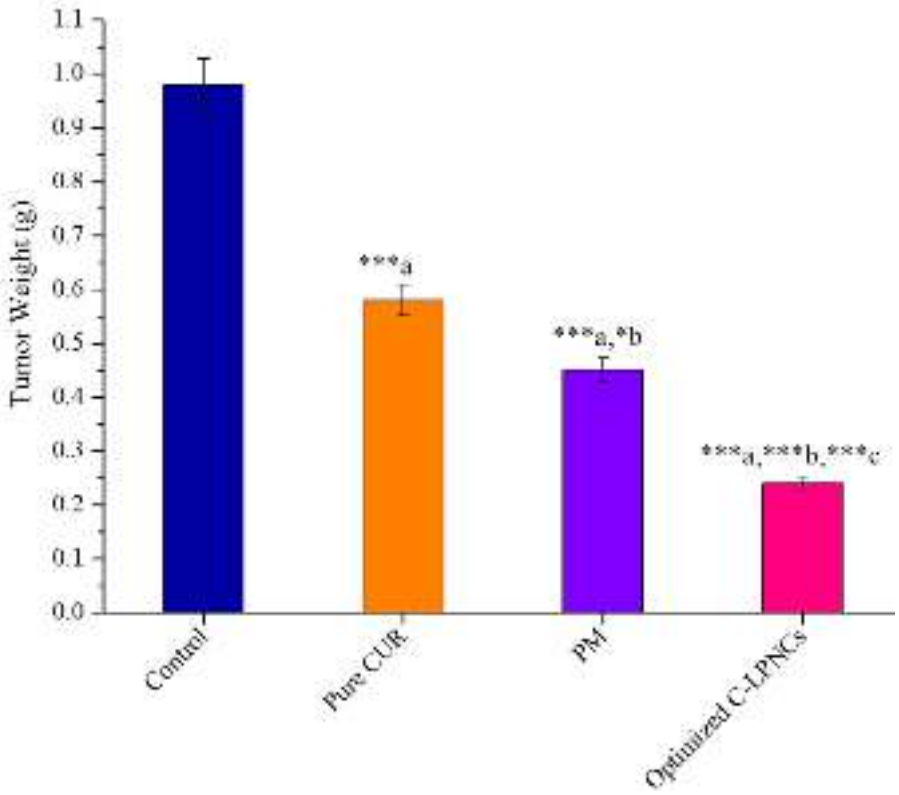

Figure 6.19 Tumor weight of each groups at the end of the test (i.e. after 30 days of dose administration observation);
Vertical bars represent ±SEM; n=6.
(*p<0.001, *p<0.05 a vs control, b vs pure CUR and c vs PM; One-way ANOVA followed by Tukey's multiple comparison test).**

These above results indicated that optimized C-LPNCs may passively be targeted into the tumors via a phenomenon termed as EPR effect (Maeda *et al.,* 2000). Due to the "leaky vasculature" of solid tumor, circulating C-LPNCs diffuse preferentially into tumor tissues. Long circulation is an essential desirable property, which can prevent fast elimination of drug and provide sufficient time for accumulation of maltodextrin based C-LPNCs in the form of "cancer nets" around tumors and retard their growth, which in turns depends on the PS (Wong *et al.,* 2008). The tumor vascular and inflamed tissues exhibit larger pore cut-off size that varies between 200 and 780nm, depending on the tumor type (Torchilin, 2007). The PS of the optimized C-LPNCs was found to be <115nm in

the present study. Therefore, there was an upper limit placed upon the size of the nanocarriers, permitting diffusion through the vascular tumor pores (Fang *et al.,* 2011). Furthermore, the oral administration of optimized C-LPNCs showed enhance survival time of tumor-bearing mice. These observations also hint that the higher build-up of the drug concentration might have happened in a discriminating manner in tumor tissue.

PART 2

6.1.3 Formulation, optimization and evaluation of CUR encapsulated eudragit E 100 nanoparticles (CENPs) *in-vitro* and *in-vivo*

6.1.3.1 Preparation of physical mixture

The physical mixture (PM) in an equimolar ratio (1:1:1) was prepared manually by mixing CUR, Eudragit E100 (EE100) and PLX188 thoroughly for 10 min in a mortar using pestle until a homogeneous mixture was obtained. The sample was passed through 40# mesh and stored in a desiccator till further use.

6.1.3.2 Preparation of CENPs

The formulation of CENPs were prepared by the emulsification-diffusion-evaporation method with little modification (Fessi *et al.,* 1989) using drug-polymer ratio, amount of ethyl acetate, homogenization speed and PLX188 concentration. Briefly, CUR and EE100 were dissolved in ethyl acetate and stirred magnetically (IKA®, C-MAG, HS7, Germany) for 5 min. This organic solution was subsequently added into 50 ml aqueous PLX188 solution with a syringe at a distance of ~4 cm above the surface of external aqueous phase drop by drop under homogenization speed (IKA® T25 digital ULTRA-TURRAX®, Germany) for 10 min. Thereafter, 25 ml of water was added into final emulsion to allow diffusion of the organic solvent into water followed by magnetically stirred at room temperature for 24 hr, to evaporate the residual organic solvent, leading to the formation of CENPs. Further, the prepared CENPs were centrifuged at 15000 rpm for 30 min. The schematic representation of formation of CENPs along with main step of preparation is shown in Figure 6.20. The sediment was washed, resuspended in distilled water containing 2% w/v mannitol as cryoprotectant and lyophilized. Finally, the lyophilized CENPs were stored in glass vessels to avoid photolytic decomposition and kept protected from light.

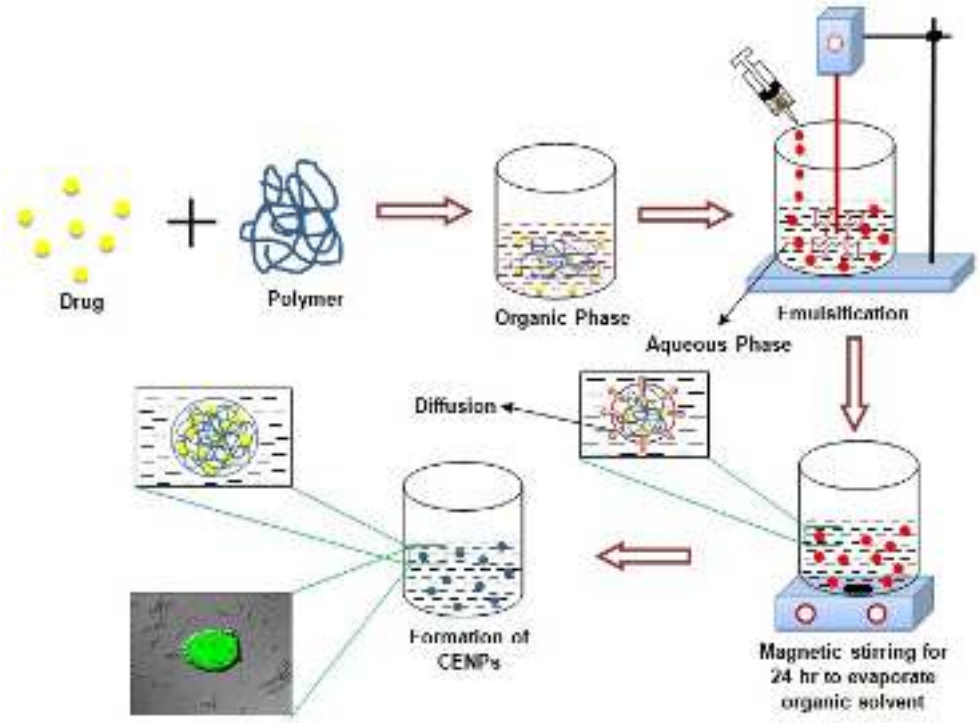

Figure 6.20 Schematic diagram showing formation of CUR loaded Eudragit E 100 nanoparticles (CENPs).

6.1.3.3 Characterization studies

6.1.3.3.1 Mean particle size, polydispersity index and zeta potential

Physicochemical characterizations viz. mean particle size, polydispersity index and zeta potential of prepared CENPs were performed as same protocol as described in ***Sub-section 6.1.1.3.1.***

6.1.3.3.2 Entrapment efficiency (EE) and drug loading (DL)

The %EE and %DL of prepared CENPs was estimated by using direct method. The procedure for estimation of %EE and %DL are same as described in ***Sub-section 6.1.1.3.2.***

6.1.3.4 Design of experiment and statistical analysis

6.1.3.4.1 Software

The same software was used to optimized the prepared CENPs as mentioned in ***Sub-section 6.1.1.4.1.***

6.1.3.4.2 TOED and crossed array layout

A L_9 (3^4) TOED (Taguchi, 1986; Rao *et al.,* 2008) was used in the current study to define the optimal conditions regarding the selected independent factors to produce nanoparticles with minimal PS, high %EE and required ZP. The robust design used to examine four independent factors each in three levels as shown in Table 6.8. The L and subscript 9 denote the Latin square and the number of the experimental runs, respectively. A run involved the corresponding combination of levels to which the factors in the experiment were set. The factors were drug-polymer ratio, amount of ethyl acetate, homogenization speed and PLX188 concentration. As shown in Table 6.9, the L_9 (3^4) array had 9 rows and four columns at three levels. Each of the nine experiments was performed in triplicate, corresponding to a total of 27 tests to reduce experimental errors (Waddada *et al.,* 2013). Three major tools used in the Taguchi method are the orthogonal arrays, analysis of variance and the mean response/signal-to-noise ratio(S/N). The rest of the description was same as mentioned in ***Sub-section 6.1.1.4.2.***

Table 6.8 Independent factors and their corresponding levels of TOED (4-factors, 3-levels)

Independent Factors	**Levels**		
	Low (1)	**Medium (2)**	**High (3)**
A: Drug: Polymer Ratio	1:4	1:6	1:8
B: Amount of Ethyl Acetate (ml)	2.5	5.0	7.5
C: Homogenization speed (rpm)	8000	10000	12000
D: PLX188 concentration (%w/v)	0.5	1.0	1.5

Table 6.9 Taguchi L_9 (3^4) orthogonal Arrays

Batches	A	B	C	D
CEEI	1:4	2.5	8000	0.5
CEEII	1:4	5.0	10000	1.0
CEEIII	1:4	7.5	12000	1.5
CEEIV	1:6	2.5	10000	1.5
CEEV	1:6	5.0	12000	0.5
CEEVI	1:6	7.5	8000	1.0
CEEVII	1:8	2.5	12000	1.0
CEEVIII	1:8	5.0	8000	1.5
CEEIX	1:8	7.5	10000	0.5

Where, A: drug:polymer ratio; B: amount of ethyl acetate (ml); C: homogenization speed (rpm); D: PLX188 concentration (%w/v)

6.1.3.4.3 Analysis of Variance (ANOVA)

The same procedure is used as mentioned in ***Sub-section 6.1.1.4.3.***

6.1.3.5 Solid state characterization

6.1.3.5.1 Fourier transform infrared spectroscopy study

The pure CUR, EE100, PM and optimized CENPs were characterized by using same instrument and protocol as mentioned in ***Sub-section 6.1.1.5.1.***

6.1.3.5.2 Differential scanning calorimetric study

The DSC thermograms of pure CUR, EE100, PM and optimized CENPs was evaluated by using same instrument and protocol as mentioned in ***Sub-section 6.1.1.5.2.***

6.1.3.5.3 Powder X-ray diffraction study

The Powder X-ray diffraction patterns of pure CUR, EE100, PM and optimized CENPs was obtained by using same instrument and protocol as mentioned in ***Sub-section 6.1.1.5.3.***

6.1.3.6 Morphological evaluation

6.1.3.6.1 High resolution transmission electron microscopy study

The surface morphology of the optimized CENPs was studied using same instrument and protocol as described in ***Sub-section 6.1.1.6.1.***

6.1.3.6.2 Atomic force microscopy study

The shape and size distribution of optimized CENPs was characterized by using same instrument and protocol as described in ***Sub-section 6.1.1.6.2.***

6.1.3.7 Evaluation of drug distribution within the polymeric nanoparticles

The distribution of CUR within the polymeric nanoparticles (PNs) was examined by using same instrument as described in ***Section 6.1.1.7.***

6.1.3.8 Analysis of photophysical properties

Entrapment of CUR into the core of PNs was further examined by UV-Visible spectroscopic analysis (Sahu *et al.,* 2008). The method of examination are same as described in ***Section 6.1.1.8.***

6.1.3.9 *In-vitro* drug release study

Dialysis bag diffusion technique was used to study *in-vitro* release of CUR from the prepared CENPs in PBS, pH 7.4. The procedure is same as mentioned in ***section 6.1.1.9.***

6.1.3.10 Stability study

The protocol for stability study is same as described in ***section 6.1.1.10.***

6.1.3.11 *In-vivo* pharmacokinetic study

6.1.3.11.1 Animals

The animal details are discussed earlier in ***Sub-section 4.1.3.1.***

6.1.3.11.2 Dosing and sampling

The dosing and sampling for optimized CENPs are same as described in ***Sub-section 6.1.1.11.2.***

6.1.3.11.3 Chromatography conditions and drug extraction

The details of chromatography conditions and drug extraction are mentioned in ***Sub-section 5.1.1.3.1 and 5.1.1.3.3***, respectively.

6.1.3.11.4 Pharmacokinetic parameters

The pharmacokinetic parameters for all CUR formulations are determined by same software as mentioned in ***Sub-section 6.1.1.11.4.***

6.1.3.12 Cell culture experiments

6.1.3.12.1 Cells

The details of cells and their culture conditions are explained in ***Sub-section 4.1.3.2*.**

6.1.3.12.2 *In-vitro* cytotoxicity study

The *in-vitro* cytotoxicity study of all CUR formulations was determined by the same assay as described in ***Sub-section 6.1.1.12.2.***

6.1.3.13 *In-vivo* anticancer activity

In-vivo anticancer activity was evaluated using same tumor-bearing mice as mentioned in ***section 6.1.1.13.***

6.1.3.14 Statistical analysis

The statistical analysis was performed with same software as described in ***section 6.1.1.14.***

6.1.4 RESULTS AND DISCUSSION

6.1.4.1 Preparation of CENPs by emulsification-diffusion-evaporation method

The preparation of CENPs by emulsification-diffusion-evaporation method was first developed by Fessi *et al.,* 1989. The preparation of CENPs require three steps: organic, aqueous and dilution. The organic phase consists a

solution of polymer and active substance in an organic solvent which is partially miscible with water. The aqueous phase (purified water) comprises the aqueous dispersion of a stabilizing agent (PLX188) while the dilution phase is usually purified water.

There are two mechanisms involved for this method, first is based on the Marangoni effect (mechanical mechanism). In this, strong interfacial tension gradients cannot be driven by variations of interfacial concentrations of organic solvent and aqueous phase since organic solvent used is partially water-miscible, mutual saturation of the phases is required in order to obtain an emulsion in thermodynamic equilibrium. Once the emulsion is formed, the submicron droplets are then diluted in water and interaction between the emulsion droplets and dilution phase is referred to as a "modification of phase equilibrium and solvent diffusion", which leads to polymer precipitation since the polymer is in organic solvent (Quintanar *et al.,* 1998; Know *et al.,* 2001). In addition, higher stabilizing agent concentrations are used (usually 1.5% 1.0% and 0.5%, respectively) which could drastically reduce the interfacial phenomena that govern the break up of emulsion globules. The second approach is based on the fact that the PNs are formed after solvent diffusion from an emulsion droplet. The mean particle size is always smaller than that of the emulsion droplets. Thus emulsion droplet size governs final particle size and consequently, it is directly influenced by all the operating variables linked to the preparation of the emulsion and their colloidal properties. The way emulsion droplets in the organic phase are formed can be explained by binary break-up mechanisms (Briscoe *et al.,* 1999). In this mechanism, droplets are continuously broken up into two fragments, until the drop size is small enough to survive the prevailing hydrodynamic conditions.

Ethyl acetate (ICH, class 3 solvent) was selected for the preparation of organic phase as it is less toxic and of lower risk in comparison to chlorinated solvents, methanol and dichloromethane according to ICH Q3C (R4) guidelines.

Also, CUR and EE 100 showed good solubility in ethyl acetate. In addition, it is volatile in nature and does not form azeotropic mixture with aqueous phase; hence, gets easily evaporated causing minimum contamination to the PNs formulation. Therefore, PNs formulation can safely be used for further studies such as PS, PDI, ZP, EE, DL, solid state characterization, qualitative studies, *in-vitro* and *in-vivo* studies.

6.1.4.2 Characterization studies

6.1.4.2.1 Mean particle size, polydispersity index and zeta potential

The effect of PLX188 concentration and homogenization speed on the PS was evaluated by varying the concentration from 0.5% to 1.5% (w/v) and speed from 8000 to 12000 rpm, respectively. The results showed that when PLX188 concentration was increased from 0.5% to 1.5% (w/v), the emulsion droplets with the PS decreased from 688.23 (Batch CEEIX) to 248.40 nm (Batch CEEIII), as shown in Table 6.10. The formation of smaller PS of CENPs was due to the effect of high concentration of PLX188, which leads to the droplet formation mechanism. Thus, PLX188 was adsorbed on the organic-aqueous interfacial area formed during the emulsification step, while the remaining quantity contributes towards preventing CENPs aggregation in the dilution step (Know *et al.,* 2001). In addition, the steric effects are also important for preventing polymer aggregation. The behavior of the PNs obtained confirms that efficient reduction of interfacial tension combined with steric effects permit to obtained smaller PS. Consequently, the high homogenization speed lead to exhaustive fragmentation in the organic-aqueous phases, formation of small emulsion droplets followed by small PS obtaining (Poletto *et al,* 2008). The PDI value allows us to determine the level of homogeneity between different sizes of CENPs. The small value of PDI (<0.25) indicates a homogeneous CENPs formulation, whereas a larger PDI (>0.3) indicates heterogeneity. The PDI values of different batches were found in the range from 0.212 (Batch CEEIII) to 0.712 (Batch CEEIX), as shown in Table

6.10. The batch CEEIII exhibited PDI value <0.25 indicating homogeneous CENPs formulation. The ZP constitutes an important parameter for determining the physical stability of a colloidal dispersion. The electrophoretic mobility measurements and subsequent calculation of ZP in the samples revealed that nanoparticles formulation showed positive/negative ZP values. Therefore, the prepared CENPs using cationic polymer (EE 100) and non-ionic stabilizing agents, exhibited positive zeta-potential values due to the presence of polymer terminal carboxylic groups. The values of ZP were found to be in the range of +28.9 (Batch CEEIII) to +14.3 mV (Batch CEEIX) as shown in Table 6.8. Large absolute values of ZP indicate the presence of a high electric charge on the PNs surface, and hence more stable formulations (Yousefi *et al.,* 2009).

6.1.4.2.2 Entrapment efficiency and drug loading

Table 6.10 shows %EE and %DL for the prepared CENPs formulation. The aqueous PLX188 solution was used as an external phase to avoid CUR degradation during encapsulation process. The number of formulation parameters such as drug/polymer ratio, organic phase (internal phase) and aqueous phase (external phase) were modified to achieve CENPs with acceptable %EE and %DL. The highest %EE values were found to be in the range of 55.33% (Batch CEEIX) to 75.93% (Batch CEEI) while the %DL varied from 0.455% (Batch CEEIX) to 1.786% (Batch CEEI), and was attributed to better drug/polymer affinity (Mittal *et al.,* 2007). At better drug/polymer ratio the viscosity of organic phase (ethyl acetate) increases which ultimately decreases the net shear stress during emulsification which formed larger droplets. With this decreased drug diffusion into external aqueous phase, it resulted in more entrapment of CUR. On the other hand, higher value of organic-aqueous affinity lead to increased restoring stress and interfacial tension of the emulsion droplets which resulted in formation of large size of the emulsion droplets during emulsification process which is unfavourable for organic phase diffusion to external aqueous phase (Sahana *et al.,* 2008), and it resulted into better EE and DL.

Table 6.10 Physicochemical parameters; PS, ZP, PDI, %EE and %DL of various batches (All values reported are mean±SD; n = 3)

Batches	PS(nm)	ZP(mV)	PDI	%EE	%DL
CEEI	611.40±2.56	16.4±2.09	0.632±0.07	75.93±1.93	1.786±0.045
CEEII	546.50±3.24	21.1±1.19	0.598±0.04	69.81±2.88	0.872±0.036
CEEIII	248.40±3.89	28.9±0.47	0.212±0.013	65.77±3.17	0.559±0.026
CEEIV	362.80±5.22	22.3±3.17	0.432±0.032	72.13±2.92	1.621±0.065
CEEV	488.45±1.25	17.9±0.97	0.502±0.041	63.09±2.28	0.769±0.027
CEEVI	408.40±2.78	19.2±1.01	0.482±0.05	60.12±3.60	0.503±0.030
CEEVII	302.23±3.12	25.7±2.07	0.382±0.08	70.72±0.97	1.521±0.021
CEEVIII	342.50±1.87	23.3±1.97	0.412±0.062	61.68±2.21	0.734±0.026
CEEIX	688.23±1.67	14.3±1.61	0.712±0.093	55.33±1.62	0.455±0.013

Where; PS: mean particle size; ZP: zeta potential; PDI: polydispersity index; %EE: percent entrapment efficiency; %DL: percent drug loading

6.1.4.3 Design of experiment and statistical analysis

6.1.4.3.1 Formulation optimization using TOED

TOED is one way to qualitatively analyze the correlations between relevant variables at different levels by designing an orthogonal table and performing statistical analysis based on the different process parameters, an orthogonal experimental design at four factors and three levels [L9 $(3)^4$] was performed to optimize the formulation compositions (Cui *et al.,* 2007). The formulation composition and their corresponding levels are given in Table 6.8. The dependent variables considered were PS and %EE. The range of PS and %EE observed from the orthogonal experimental runs were 248.40 to 688.23 nm and 55.33 to 75.93%, respectively. However, we could not select the optimum formulation composition based only on these results as shown in Table 6.10, therefore; further orthogonal analysis was warranted for each response. Thus, the PS_i, EE_i and delta values were calculated for each response. In Table 6.11, the factors influencing the mean PS are listed in decreasing order as follows D>C>A>B according to the delta value. In addition, the influences on the PS at individual levels within each factor are explained by PS_i values and can be

ranked as: A: 2>3>1; B: 1>3>2; C: 3>1>2; D: 3>2>1 as shown in Figure 6.21a. The optimum formulation should be $A_2B_1C_3D_3$. Similarly, the sequence of factors influencing the %EE was in order, B>A>D>C based on the delta value and the individual levels within each factor are ranked as: A: 1>2>3; B: 3>2>1; C: 2>1>3; D: 1>3>2 as shown in Figure 6.21b. The highest %EE could be obtained at $A_1B_3C_2D_1$, signifying that both of these responses cannot have their desired values at the same variable setting. ANOVA results along with delta value suggested that factors C and D were highly significant in determining PS with a P value of 0.009 and 0.002, respectively at 95% confidence level. Thus, other two factors can be arbitrarily effect on the response. Factors A and B, with P values of 0.006 and 0.001, respectively at 95% confidence level, were found to have their highest effects on %EE as shown in Table 6.12. Therefore, the level settings C_3D_3 and A_1B_3 were significant importance for the PS and %EE, respectively. Thus, PS and %EE of the CENPs was considered to be relatively more important response parameters and therefore, the final stastically optimized CENPs formulation was established as 1:4 (w/w) CUR/EE100 ratio, 7.5 ml ethyl acetate, 12000 rpm homogenization speed and 1.5% w/v PLX188 concentration i.e. batch CEEIII.

Table 6.11 Experimental mean value for the response parameters at different levels of prepared CENPs according to TOED

Levels	**Independent Factors**			
	A	**B**	**C**	**D**
PS_1	236.0	214.6	228.3	298.9
PS_2	211.5	230.6	267.9	211.0
PS_3	223.3	225.6	174.6	160.8
Delta value	24.5	16.0	93.3	138.1
Rank	3	4	2	1
EE_1	32.09	37.44	34.25	33.37
EE_2	34.03	33.66	34.12	34.69
EE_3	36.59	31.60	34.34	34.65
Delta value	4.50	5.84	0.22	1.32
Rank	2	1	4	3

PS_i and EE_i is the mean value of PS and EE.
Delta value is the difference between the maximum value and the minimum value of PS_i and EE_i.

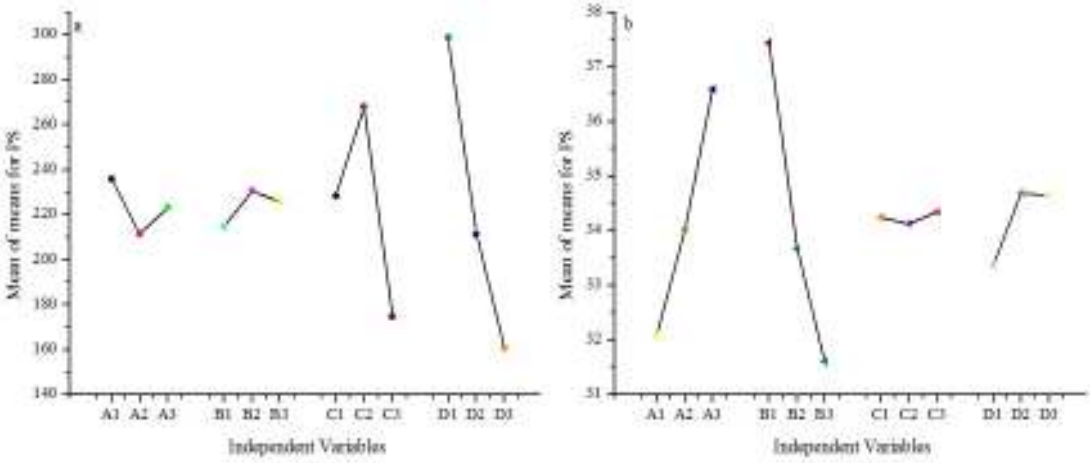

Figure 6.21 Marginal mean graphs of the mean for (a) PS and (b) EE

Table 6.12 ANOVA table for the response parameters of PS and EE

Factors	DoF	SS	MS	%PC	F[a]	P[b]
PS						
A	(2)	(52408)	(26204)	29.664	pooled	
B	(2)	(118908)	(59454)	67.303	pooled	
C	2	3484	1792	2.029	0.0406	0.009
D	2	1774	887	1.004	0.0207	0.002
Pooled Error	(4)	(171316)	(85658)			
SS_{Total}	8	176674		100		
%EE						
A	2	1.012	0.506	28.189	0.0059	0.006
B	2	7.542	3.771	69.357	0.0443	0.001
C	(2)	(98.319)	(49.1595)	0.2902	pooled	
D	(2)	(241.904)	(120.952)	2.163	pooled	
Pooled Error	(4)	(340.223)	(170.1115)			
SS_{Total}	8	348.777		100		

DoF; degree of freedom, SS; sum of squares, MS; mean of squares, %PC; percent contribution, F; fisher test

[a] $F_{0.05}$ *(2,4)=6.94*

[b] *P<0.05; significant in C and D for PS and in A and B for %EE.*

6.1.4.4 Solid state characterization

6.1.4.4.1 Fourier transform infrared spectroscopy study

The FTIR spectra for pure CUR, EE100, PM and optimized CENPs are shown in Figure 6.22. The FTIR spectrum of pure CUR (Figure 6.22a) shows characteristic absorption bands at 3,489 cm^{-1} which represent phenolic –OH group, at 1,629 cm^{-1} the C=O stretching peak of conjugated ketone, at 1,371-1,390 cm^{-1} the stretching and deformation of methyl groups, at 1,525 and 1,444 cm^{-1} represents aromatic and aliphatic C=C stretching, respectively, and the C–O–C stretching peak of ether at 1,028 cm^{-1} (Pan *et al.,* 2006). The FTIR spectra for EE100 (Figure 6.22b) show characteristic absorption bands at 2,858 cm^{-1}, which represent the presence of $-CH_2$ symmetric stretching, at 1,728 cm^{-1} represents C=O carbonyl stretching. In PM, shift from 3489 cm^{-1} to 3678 cm^{-1} is shown in Figure 6.22c, and the peak at 3678 cm^{-1} becomes wider, this indicates hydrogen bonding is enhanced**.** The FTIR spectra of optimized CENPs (Figure 6.22d) show disappearance of peak at 1,371-1,390 cm^{-1}. The reason for disappearance of peak may be due to encapsulation of CUR in CENPs formulation. The infrared bands at 1161 cm^{-1} and 1028 cm^{-1} could be attributed to C-O stretching and C-O-C stretching vibrations. Therefore, all of the above indicating bands were observed in optimized CENPs without changing their positions. These results indicated the chemical stability of CUR in PNs formulation and no specific interaction was observed in PM and optimized CENPs.

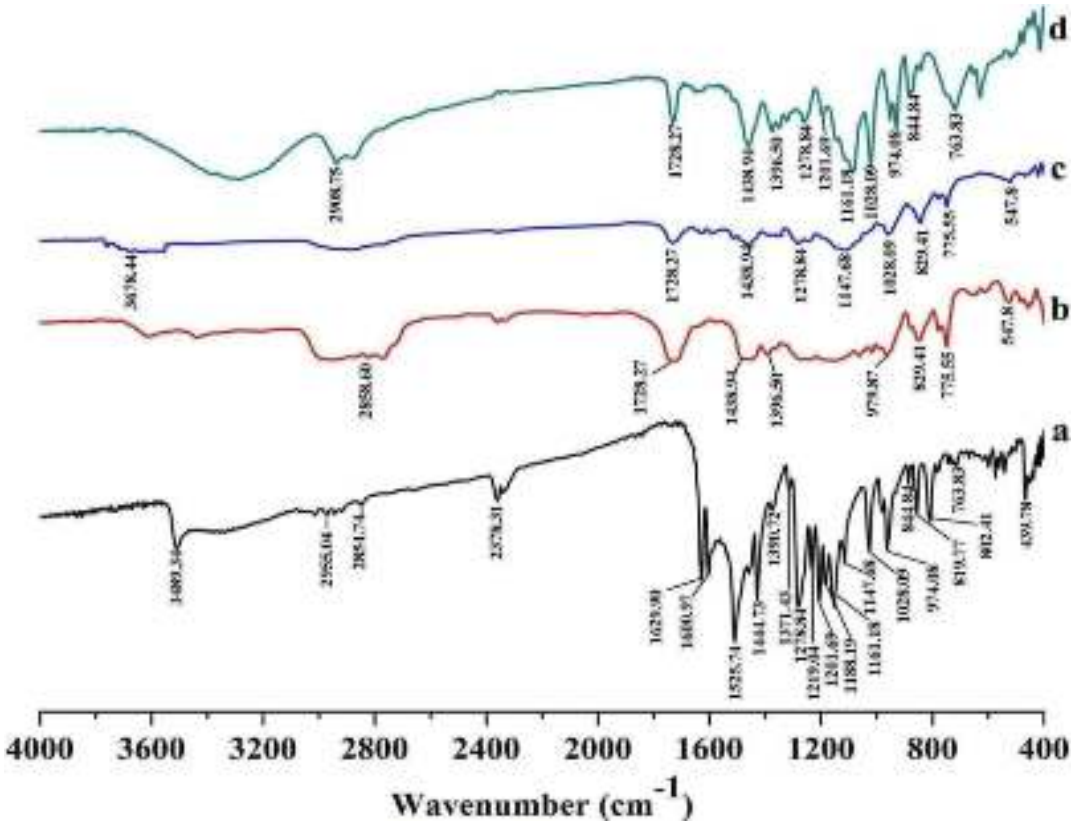

Figure 6.22 FTIR spectra of (a) pure CUR (b) EE100 (c) PM and (d) optimized CENPs.

6.1.4.4.2 Differential scanning calorimetric study

DSC thermograms of pure CUR, EE100, PM and optimized CENPs are shown in Figure 6.23. Both pure CUR and PM exhibited a melting temperature of the drug followed by a sharp exothermic decomposition peak at 180°C. However, this melting peak was not appeared in the DSC thermogram of optimized CENPs. It seemed that the CUR was encapsulated in EE100 nanoparticles as an amorphous form (Mohanty & Sahoo, 2010).

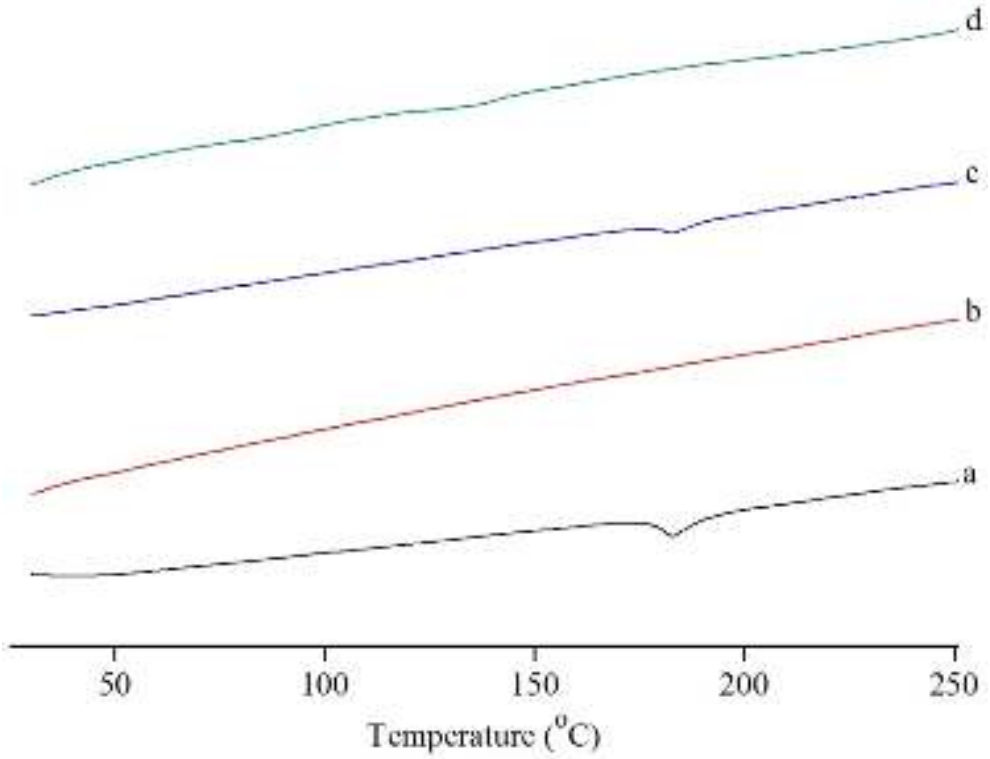

Figure 6.23 DSC thermograms of (a) pure CUR (b) EE100 (c) PM and (d) optimized CENPs.

6.1.4.4.3 Powder X-ray diffraction study

*p*XRD was used to confirm the loss of drug crystallinity. *p*XRD analysis of pure CUR, EE100, PM and optimized CENPs are shown in Figure 6.24. The Figure 6.24a shows several characteristics peaks of pure CUR at 2θ angles within 30° (Mohanty & Sahoo, 2010). The EE100 does not exhibit any characteristics peaks at 2θ angles as shown in Figure 6.24b. In case of PM, although most of the peaks disappeared, peaks at 17.5°, 22.5°, 24° and 30° were still observed as shown in Figure 6.24c. Since EE100 provided no any characteristic peak, these four peaks must originate from crystalline form of CUR. The results indicated that CUR was partially present in crystalline form in the PM. Partial melting of EE100 during PM preparation dissolved some of CUR, resulting in partial transformation into amorphous form. In case of optimized CENPs formulation the characteristic peaks of CUR completely disappeared as shown in Figure 6.24d. This indicated

that all CUR was in amorphous state in the optimized CENPs formulation which may have caused enhanced dissolution of CUR (Mohanty & Sahoo, 2010).

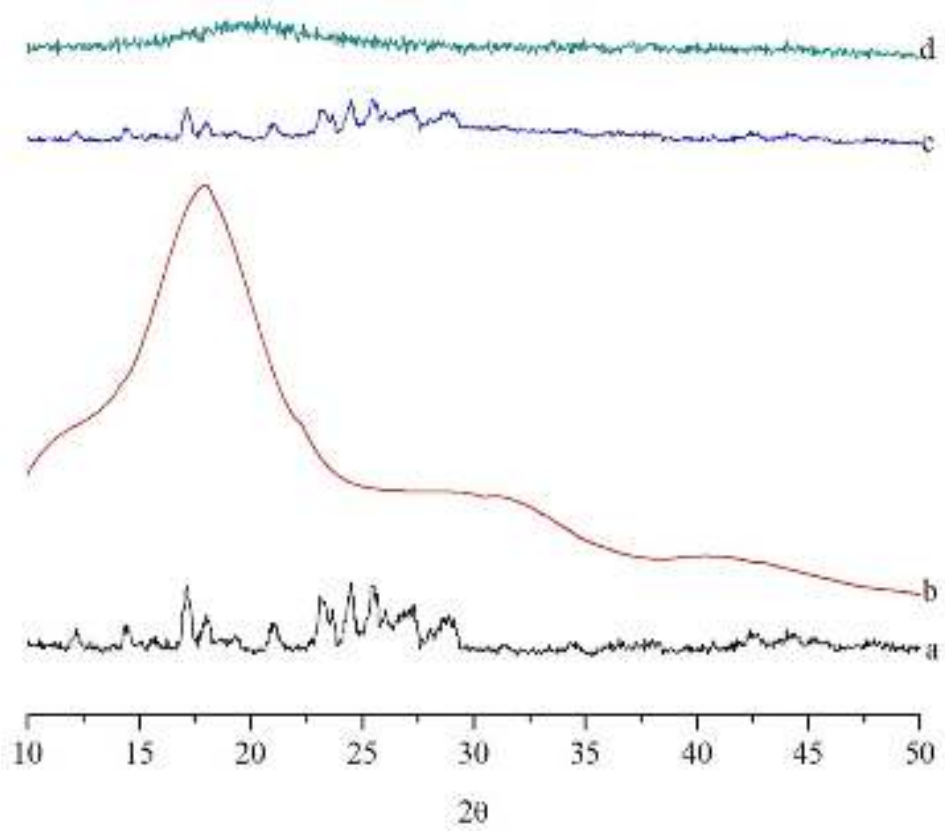

Figure 6.24 *p*XRD curves of (a) pure CUR (b) EE100 (c) PM and (d) optimized CENPs.

6.1.4.5 Morphological evaluation

6.1.4.5.1 High resolution transmission electron microscopy study

The surface morphology of optimized CENPs was determined by HR-TEM micrographs. Figure 6.25a. Illustrates TEM images showing the formation of spherical and smooth CENPs. The images also revealed that the optimized CENP have a more or less uniform size distribution and low polydispersity as represented in Table 6.10. Further, the electron diffraction (ED) pattern of optimized CENPs revealed the amorphous diffraction halo as shown in Figure 6.25b. This image clearly indicates that absence of star shaped particles in ring patterns and homogeneous distribution of drug into the matrix of PNs (Singh & Muthu, 2007).

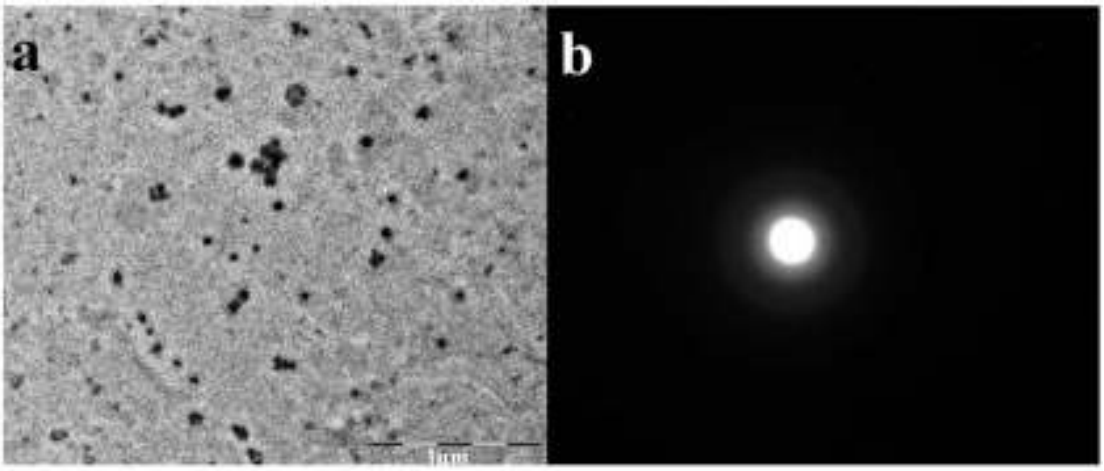

Figure 6.25 (a) HR-TEM micrographs at ×15,000 magnification (bar=1µm) and (b) electron diffraction pattern of optimized CENPs.

6.1.4.5.2 Atomic force microscopy study

The AFM micrographs of prepared CENPs exhibited well separated spherical shapes with smooth surfaces as shown in Figure 6.26 a & b. The micrographs also revealed that the CENPs have an almost uniform size distribution with low polydispersity and most of them have average diameter smaller than 300 nm as measured by particle size analyzer as depicted in Figure 6.26c.

(a)

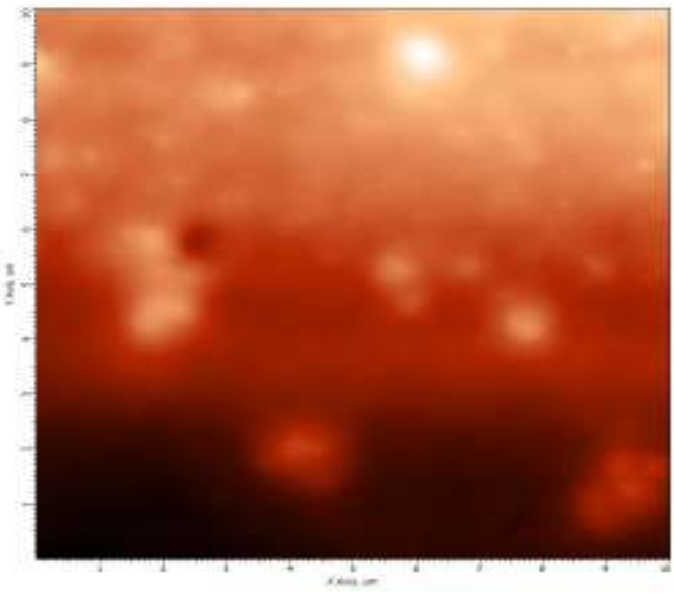

(b)

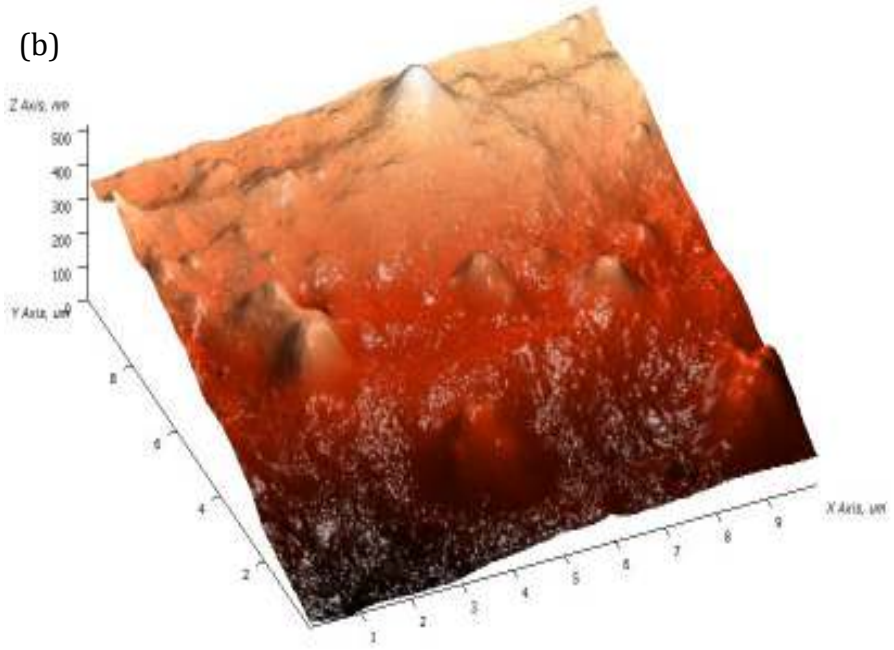

(c)

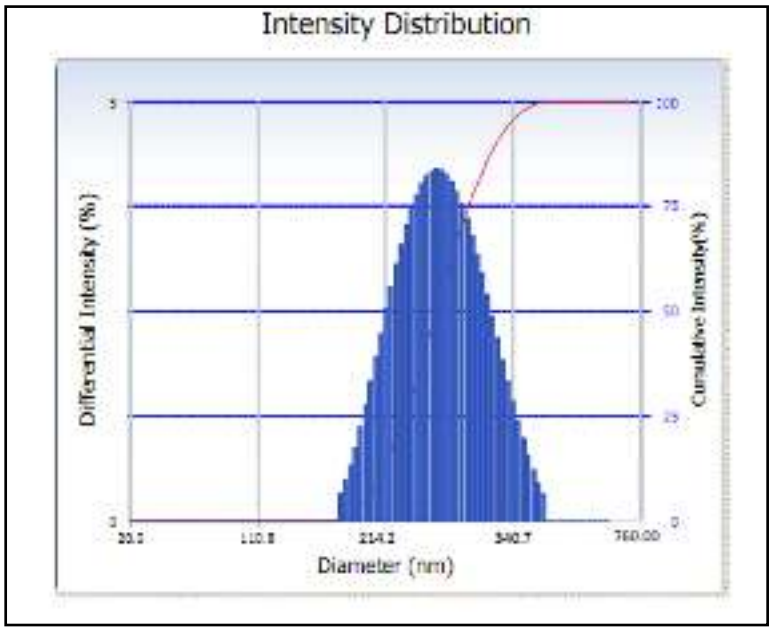

Figure 6.26 (a) Morphology of the CENPs measured by AFM (2D image), (b) corresponding 3D image and (c) Mean particle size of CENPs measured by particle size analyzer (average diameter = 248.4±3.89 nm, n=3).

6.1.4.6 Evaluation of drug distribution within the polymeric nanoparticles

The distribution of drug within the PNs was confirmed by using confocal laser scanning microscopy (CLSM) micrographs as shown in Figure 6.27. The optimized CENPs, appearing green entrapped inside the polymer matrix. The

CUR seen to be uniformly distributed within the PNs (Mukherjee & Viswanatha, 2009). This is a critical parameter that would help in uniform drug release from the PNs system once they are administered *in-vivo.*

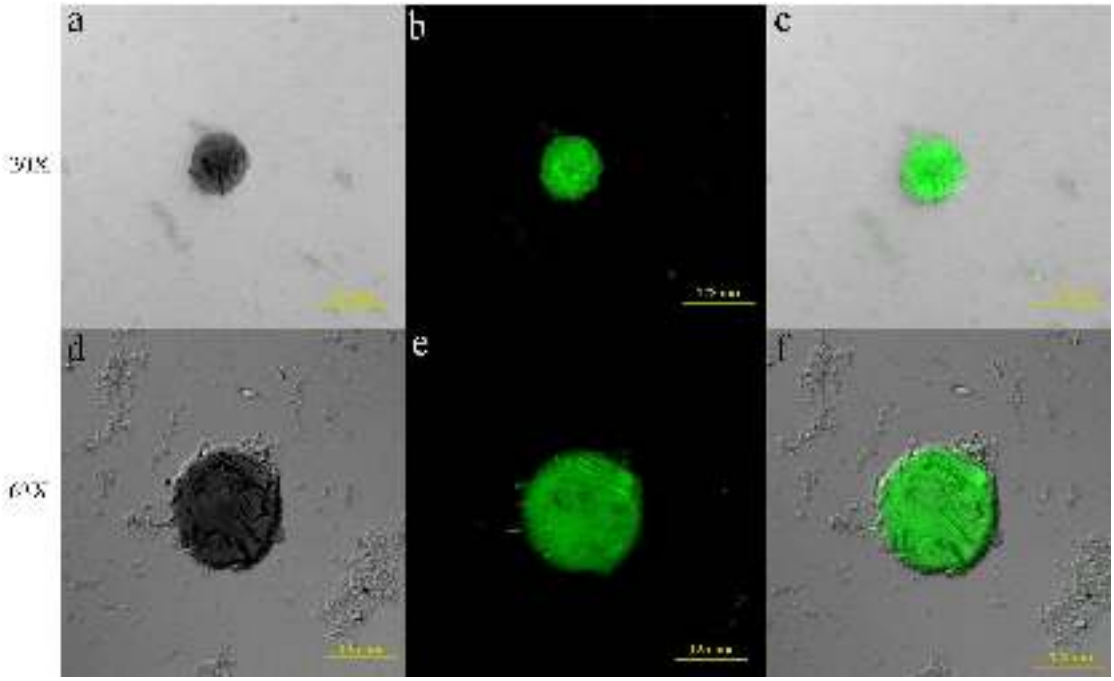

Figure 6.27 CLSM images illustrating the encapsulation and distribution of CUR (green fluorescence) within the CENPs. a and d DIC image, b and e fluorescent image, c and f merged fluorescent and DIC image at magnification 20X and 63X, respectively.

6.1.4.7 Analysis of photophysical properties

To confirm the entrapment of CUR into the core of PNs, the photophysical property of CUR was taken into consideration. Pure CUR in PBS, pH 7.4 solution showed a distinct high absorbance peak at around 420 nm. The absorbance intensity of CENPs showed less intense peak at the same wavelength of pure CUR as illustrated in Figure 6.28. This result confirms that successful incorporation of CUR into hosts such as EE100 in the form of CENPs, will increase hydrolytic stability and resistance to extensive intestinal and hepatic metabolism (Priyadarsini, 2009).

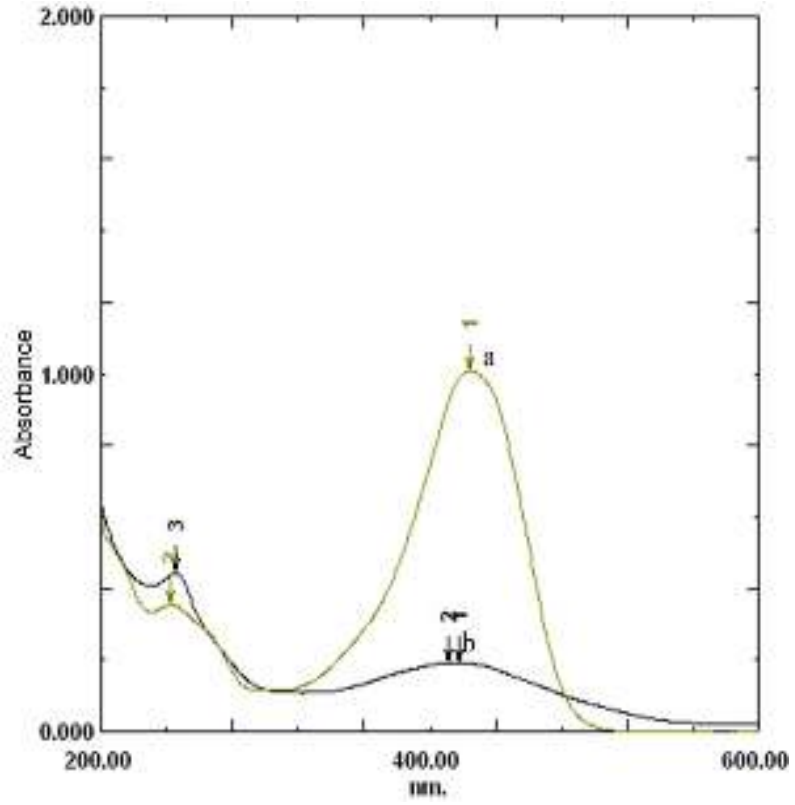

Figure 6.28 Ultraviolet-visible absorbance spectra of (a) pure CUR and (b) optimized CENPs in PBS, pH 7.4.

6.1.4.8 *In-vitro* drug release study

Figure 6.29 illustrates *in-vitro* release of pure CUR and optimized CENPs in PBS, pH 7.4 before and after 3 months storage. The pure CUR remained undissolved in PBS, pH 7.4 as compared to optimized CENPs, which gave >75% drug release at the end of 24 hr. This was due to the structural homogeneity and amorphous state of CUR in PNs which facilitate higher solubility. However, they provided burst release during first 30 min due to simultaneous release of surface bound drug (being more than 12%) followed by hydration, polymer swelling or polymer erosion of the PNs which eventually lead to diffusion based sustained drug release. Hydration brings about an increment in the diffusional path length of molecules and consequently the rate of their diffusion becomes lower (Wong *et al.,* 1999). Therefore, gaining of sustained release profile and its maintenance

could be assumed to be dependent upon the relative hydration rate of the polymer and integrity of the hydrated matrix. These results indicated that the release of CUR from EE100 nanoparticles was governed by a combination of drug diffusion and polymer chain relaxation during polymer swelling (Bhagav *et al.,* 2011).

The rate and extent of drug release might be closely related to the distribution coefficient of the drug. Furthermore, data obtained from *in-vitro* release studies of the optimized CENPs were fitted to various kinetic equations such as zero order, first order, Higuchi, Hixon-Crowel and Korsmeyer-Peppas models. The Higuchi equations were best fitted for CUR release from the optimized CENPs as indicated by a higher correlation coefficient (R^2=0.979) compared with Hixon-Crowel (R^2=0.783), first order (R^2=0.718), zero-order (R^2=0.675) and Peppas-Korsmeyer models (R^2=0.964) as shown in Table 6.13. To further elucidate the release mechanism involved in CENPs, the Korsmeyer-Peppas model was the best fit model with n value 0.499, indicating fickian diffusion mechanism of drug release from the polymer matrix (n≤0.5 for fickian diffusion) (Costa & Sousa, 2001; Korsmeyer *et al.,* 1983).

Table 6.13 Release parameters for optimized CENPs (batch CEEIII) obtained after fitting *in-vitro* drug release data to five different mathematical models for drug release kinetics

Batch	Zero order	First order	Higuchi model	Hixon-Crowel model	Korsemeyer-Peppas model
CEEIII	K_z =2.943 (Con./time) R^2=0.675	K_F=0.077 ($Time^{-1}$) R^2=0.718	K_H=16.77 R^2=0.979	K_{HC}=0.061 R^2=0.783	K_p=0.178 R^2=0.964 n=0.499

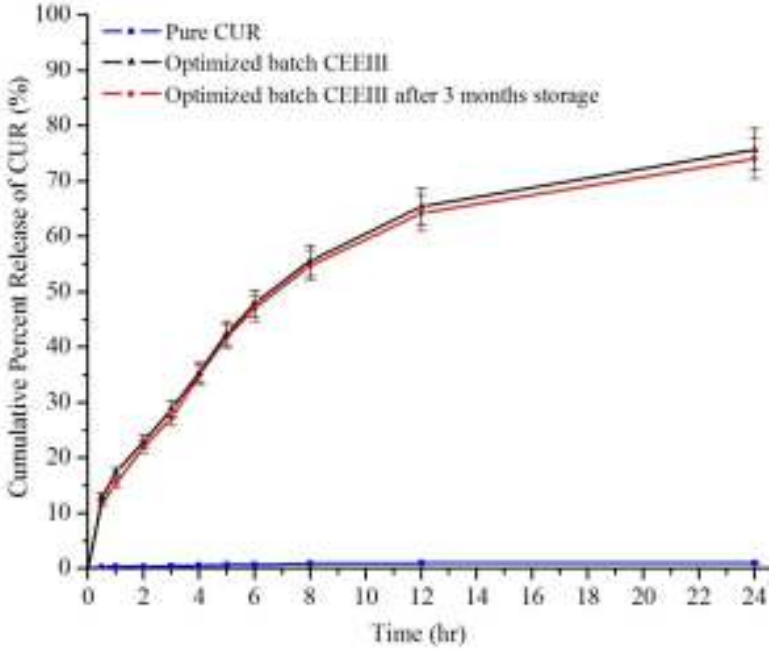

Figure 6.29 *In-vitro* release profile of pure CUR and optimized CENPs (batch CEEIII) in PBS, pH 7.4 for 24 hr before and after 3 months storage (Vertical bars represent ±SD, n=3).

6.1.4.9 Stability study

Stability studies of prepared formulations revealed that CENPs were stable over the three month study period for all the physicochemical parameters. The differences in PS, PDI and percent entrapment efficiency were insignificant throughout the stability study period indicating that the CENPs were highly stable as shown in Figure 6.30.

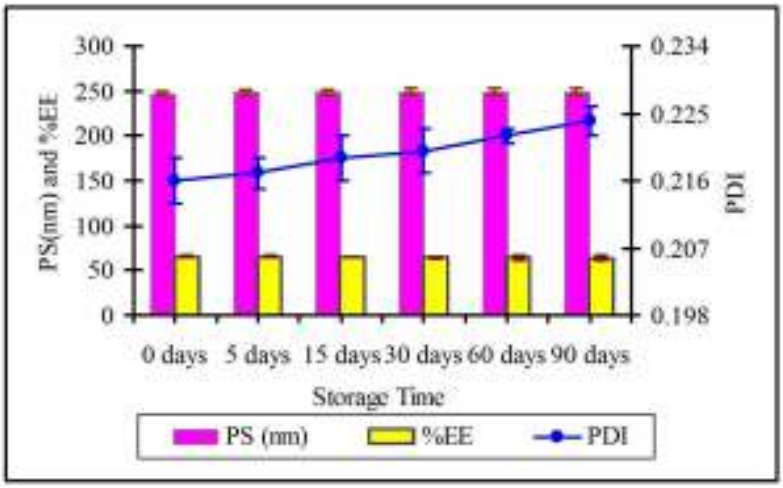

Figure 6.30 Stability data of the optimized CENPs during storage at room temperature (all experiments were performed in triplicate and the vertical bars represent ±SD, n=3).

6.1.4.10 *In-vivo* pharmacokinetic study

The mean plasma concentrations-time profiles obtained after oral administration of the pure CUR suspension, PM and CENPs are shown in Figure 6.31. The $AUC_{0\text{-}12}$ and C_{max} values were found to be 18.25-fold, 94.68-fold as well as 51.23-fold, 90.82-fold greater when CUR was administered as PM and CENPs, respectively, compared with pure CUR aqueous suspension (Table 6.14). It was also noticed that plasma levels declined sharply after 2 hr, indicating rapid systemic elimination in case of pure CUR. This was also evident by short biological half-life (1.25±0.042 hr) for pure CUR. These results thus indicated significant (p<0.05) improvement in oral bioavailability of CUR in PM as well as CENPs; though, the enhancement of oral bioavailability in case of CENPs was significantly (p<0.05) higher than that of the PM as well as pure CUR.

The bioavailability and pharmacokinetic data of CENPs were, compared with both the PM and pure CUR at the same dose level (50 mg/kg). The plasma level of CUR after the administration of pure CUR was detected only up to 12 hr of the oral administration with the C_{max} 9.582±0.391 ng/ml. The C_{max} and $AUC_{0\text{-}12}$ of the drug were further increased to 490.901±8.106 ng/ml and 423.856±13.118 (ng/ml).hr, respectively when PM was administered with the same dose. Further, the orally administered CENPs drastically increased the drug plasma concentrations (Figure 6.31). The $AUC_{0\text{-}12}$ for CENPs was also significantly increased to 2199.116±78.399 (ng/ml).hr (Table 6.14). These results clearly indicated that PM and CENPs significantly enhanced the oral bioavailability of CUR; though, the improvement of bioavailability in the case of CENPs was significantly higher than the PM (p<0.05) and was attributed to reduced particle size, increased surface area and reduced diffusion layer thickness in case of CENPs. Further, enhanced oral bioavailability of CUR from CENPs may also be attributed to: (i) amorphous or molecularly dispersed state of drug within the polymer matrices (Wang *et al.,* 2008) (ii) supersaturated condition of drug in the intestinal lumen by the use of pH-dependent carrier polymer (EE100) (Janssens *et al.,* 2010) (iii) the good bioadhesion and site-specificity of the CENPs to gastrointestinal mucosa due to EE100 polymer (Wang *et al.,* 2008).

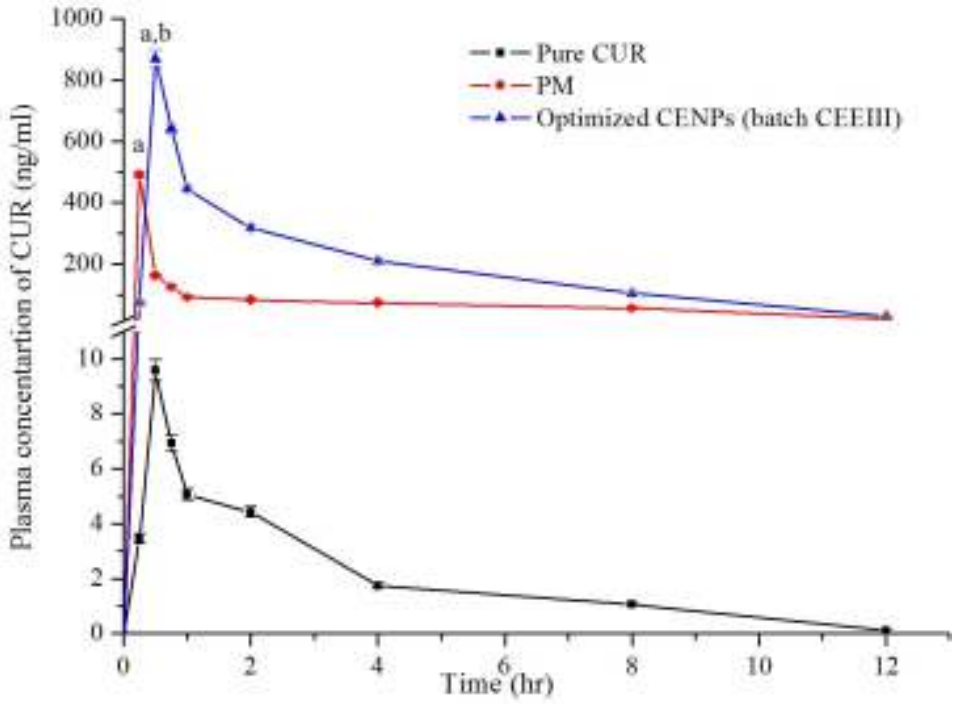

Figure 6.31 Plasma concentrations-time profile after oral administration of pure CUR, PM and Optimized CENPs (dose 50 mg/kg in each case); Vertical bars represent ±SEM; n=6.
[a]*p*<0.05, compared to the control (pure CUR)
[b]*p*<0.05, compared to PM
(One-way ANOVA; Tukey's multiple comparison test).

Table 6.14 Pharmacokinetic parameters after oral administration of PM and CENPs to rats, compared with aqueous suspension of pure CUR (dose 50 mg/kg); All values reported are mean±SEM; (n=6)

Parameters	Pure CUR (Control)	PM	Optimized CENPs
C_{max} (ng/ml)	9.582±0.391	490.901±8.106	870.3104±27.8404
T_{max} (hr)	0.5±0.0	0.25±0.0	0.5±0.0
AUC_{0-12} (ng/ml).hr	23.225±0.477	423.856±13.118	2199.116±78.399
$AUMC_{0-12}$ (ng/ml).hr^2	74.92±2.031	1472.052±51.119	12013.771±221.126
$t_{1/2}$ (hr)	1.25±0.042	2.923±0.0251	4.811±0.513
MRT (hr)	3.225±0.015	3.473±0.027	5.463±0.0701

C_{max}; maximum plasma concentration, T_{max}; time to reach maximum plasma concentration, AUC; area under the plasma drug concentration-time curve, AUMC; area under the first moment plasma drug concentration-time curve, t1/2; half life, MRT; mean residence time

6.1.4.11 *In-vitro* cytotoxicity study

The *in-vitro* cytotoxicity study of normal control, pure CUR, PM and fabricated CENPs were evaluated by assessing cell viability using colorectal cancer cell line colon-26 by SRB assay. Cells were incubated with treating increasing concentrations of CUR formulations ranging from 0.1 to 100 µg/ml, a significant (p<0.001) reduction in cell viability (%) was observed in colon-26 cancer cells (Figure 6.32) and corresponding 50% cell growth inhibition (GI_{50}) was estimated. About ~ 5.5-fold and ~ 19-fold inhibition of cancer cells growth was observed for the groups treated with PM and CENPs; though the higher inhibition of cancer cell growth was found in case of CENPs as compared to both PM and pure CUR, respectively as illustrated in Figure 6.33. Since the normal control (saline solution) did not exhibit cytotoxicity i.e. 100% cell viability, therefore the decrease in cell viability caused by optimized CENPs in colon-26 cancer cells could definitely be attributed to cytotoxic property of the released CUR in the culture medium.

The *in-vitro* cytotoxicity study and, SRB results exhibited good discrimination in GI_{50} value between pure CUR, PM and optimized CENPs, thus clearly exhibiting the key role of CENPs binding and internalization in the enhancement of cytotoxic activity. It was demonstrated that PNs rapidly escape endolysosomes and enter into the cytoplasm (Das & Sahoo, 2010). The fractions of PNs that escape the endosomal section seem to remain in the cytoplasmic compartment and release the entrapped chemotherapeutic agent in a sustained manner (Sahoo & Labhestwar, 2005). Hence, as expected, the CUR loaded polymeric nanoparticles exhibited an enhanced cytotoxic efficacy as compared to both pure CUR and PM.

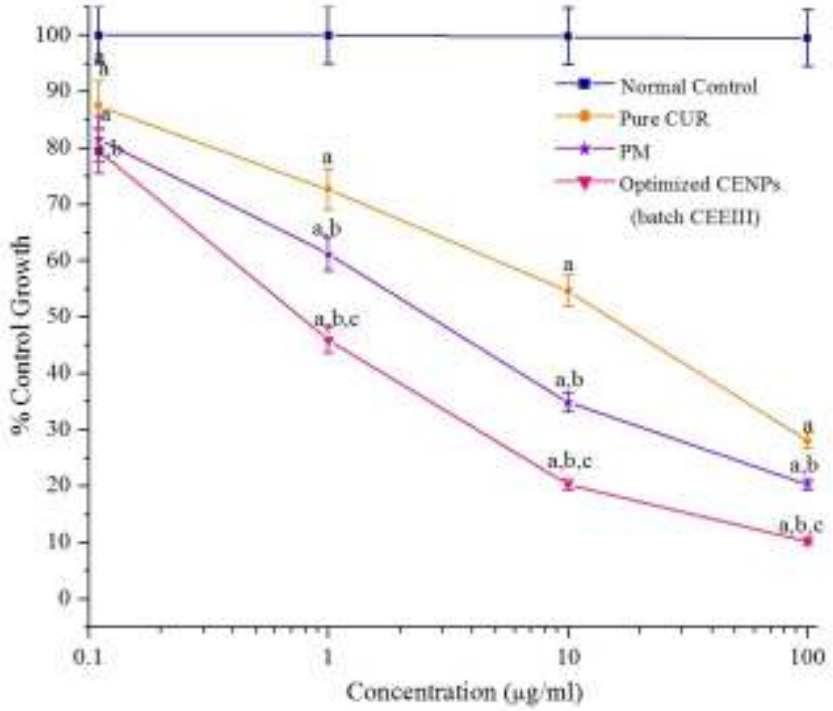

Figure 6.32 *In-vitro* cytotoxicity profile of normal control, pure CUR, PM and optimized CENPs (batch CEEIII) in colon-26 cancer cell line; Vertical bars represent ±SD; n=3; [a]*p*<0.001compared to normal control; [b]*p*<0.001 compared to pure CUR; [c]*p*<0.001 compared to PM (Two-way ANOVA; Bonferroni post hoc tests).

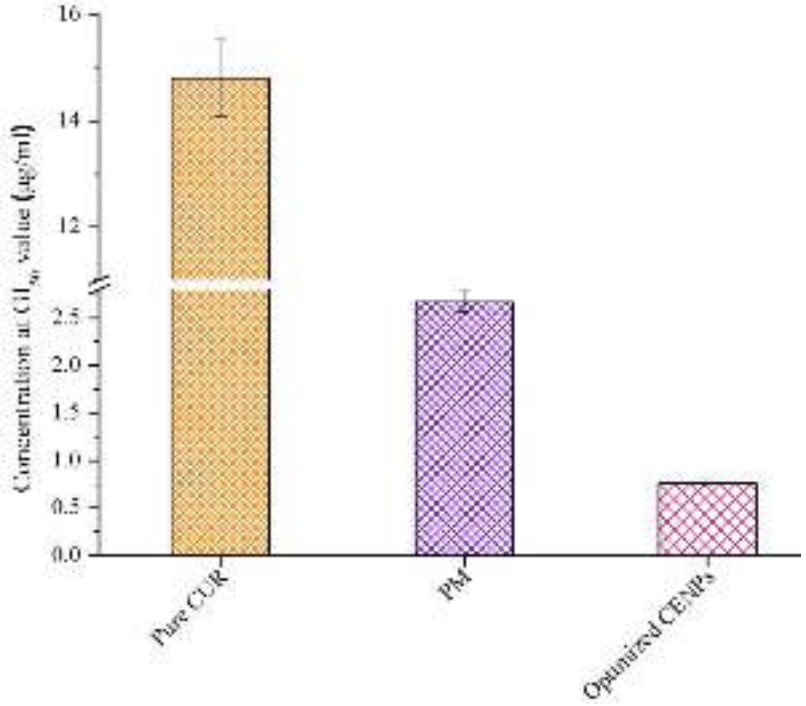

Figure 6.33 The bar chart indicating the concentrations of pure CUR, PM and optimized CENPs at GI_{50}; (Vertical bars represent ±SD; n=3).

6.1.4.12 *In-vivo* anticancer activity

The nanoparticles were further evaluated for their *in-vivo* anticancer efficacy in CRC induced animal model. Figure 6.34 shows the *in-vivo* anticancer efficacy after repetitive oral administration of pure CUR, PM and CENPs for 30 days. Tumor growth progression clearly indicates that all the formulations were able to significantly inhibit the tumor volume in comparison with control group (p<0.001) as shown in Figure 6.34a. PM resulted into significant tumor growth suppression in comparison to that of pure CUR (p<0.05); however a much higher suppression in the tumor growth was observed in case of CENPs as compared to both PM and pure CUR (p<0.001) as shown in Figure 6.34b.

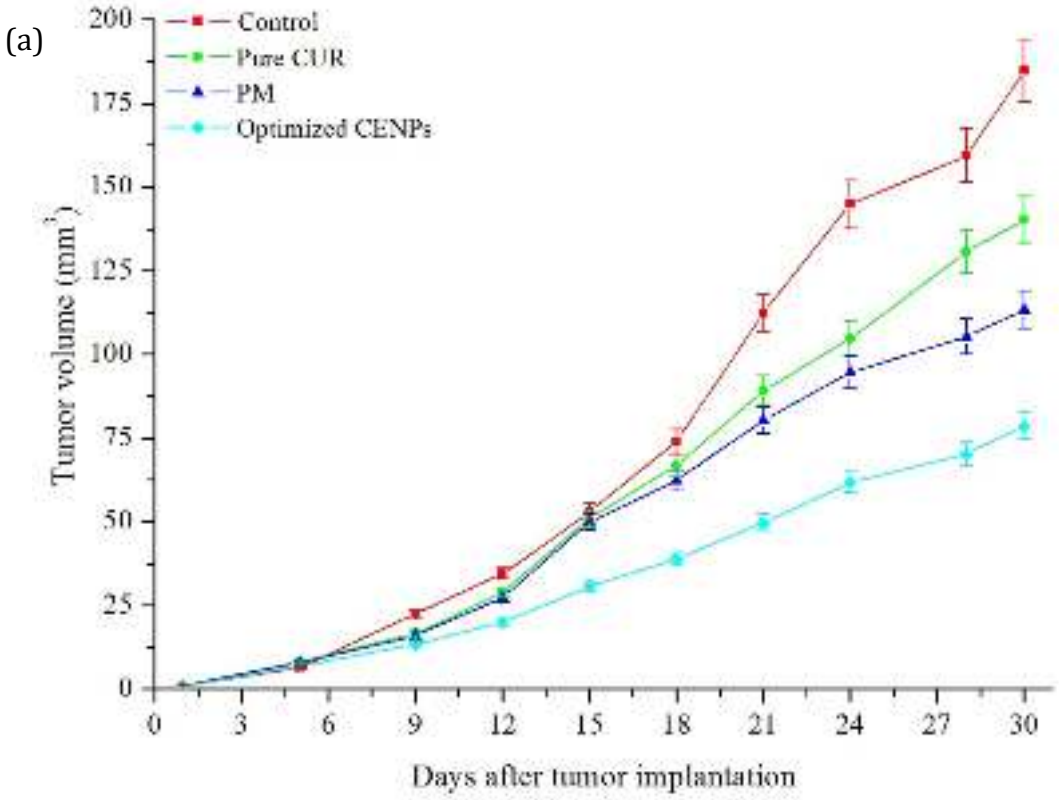

Figure 6.34 (a) Tumor progression curves for tumor-bearing mice which were orally administered with control, pure CUR, PM and optimized CENPs ([CUR]=50 mg/kg) when the tumor volume reached about ~8 mm^3 (5th day after inoculating with colon-26 cells to mice); Vertical bars represent ±SEM; n=6.

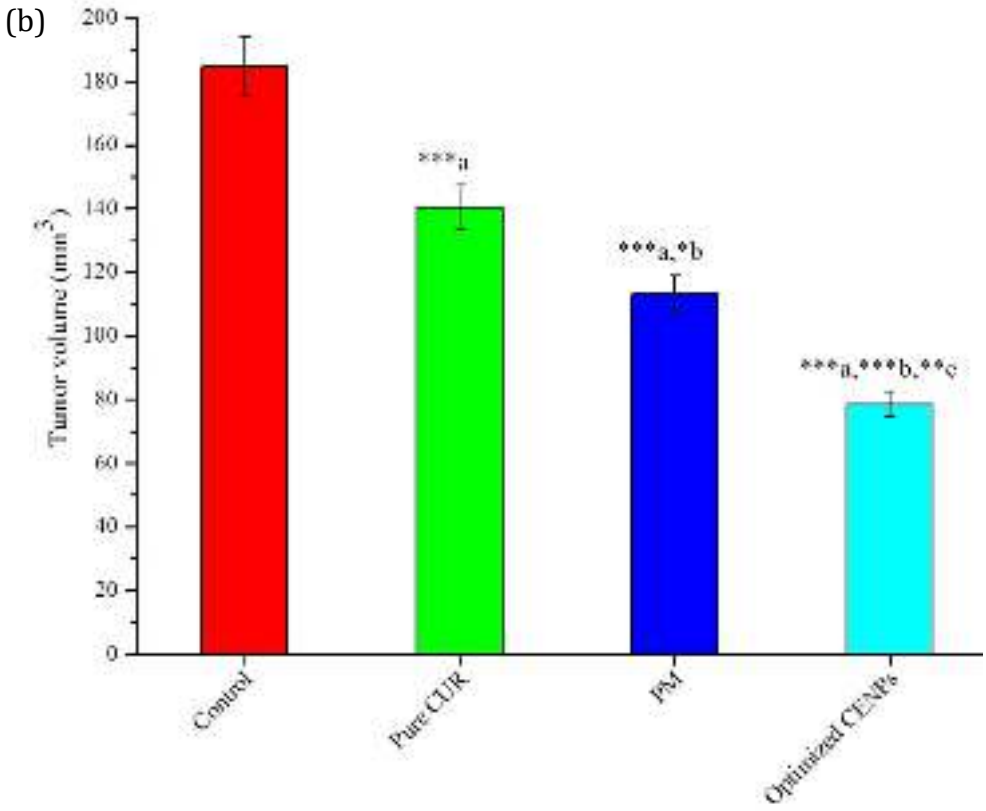

Figure 6.34 (b) Bar diagram of data from day 30 onwards from "a" part of Figure 6.33.
Vertical bars represent ±SEM; n=6.
(*p<0.001, **p<0.01, *p<0.05 a vs control, b vs pure CUR and c vs PM; One-way ANOVA followed by Tukey's multiple comparison test).**

The safety profiles of CUR formulations were evaluated by measuring the changes in body weight as a function of time as shown in Figure 6.35. A decrease in body weight was observed in control treated group of mice. The Pure CUR and PM treated group of tumor-bearing mice showed a slight increase in body weight. Whereas, CENPs treated group of mice exhibited a larger increase in body weight as compared to both pure CUR and PM treated groups.

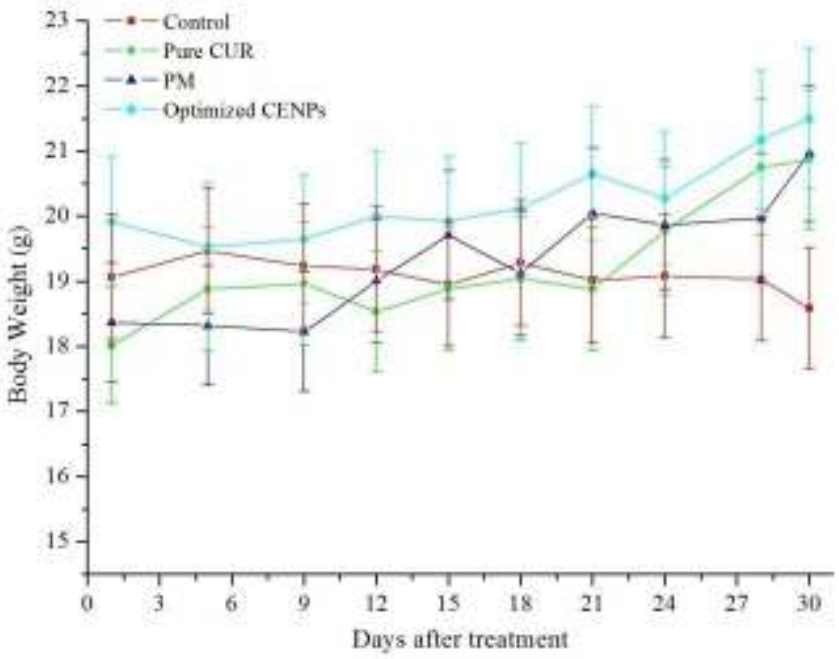

Figure 6.35 Alteration in body weight after incubation of colon-26 cells to mice and treatment with CUR formulations; (Vertical bars represent ±SEM; n=6).

The representative photographs of tumor-bearing mice from control and treatment groups at experimental end point are shown in Figure 6.36.

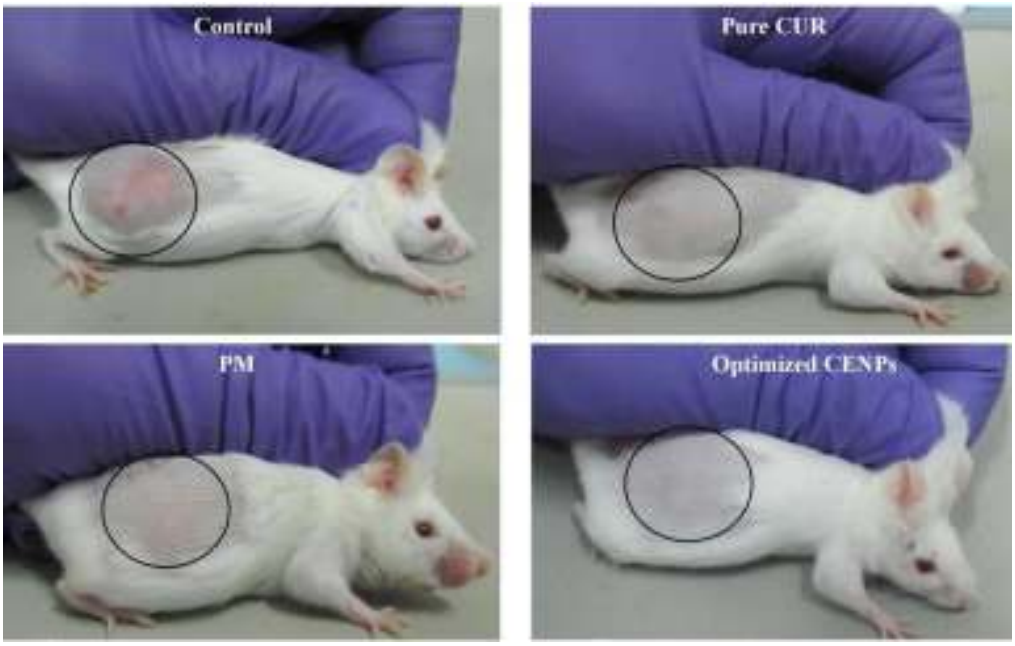

Figure 6.36 Photographs of representative tumor-bearing mice belonging to control and treatment groups at the end of 30 days of inoculation with colon-26 cells. Tumors were indicated within black circles.

Kaplan-Mirer survival plots of mice after 60 days repetitive treatment with control and different CUR formulations are depicted in Figure 6.37. The control treated group of mice showed 16.67% survival. The CENPs enhanced the survival of 83.33% of animals in 60 days as compared to PM as well as pure CUR where almost 66.67% and 33.33% survival of the animals took place at the end of the study.

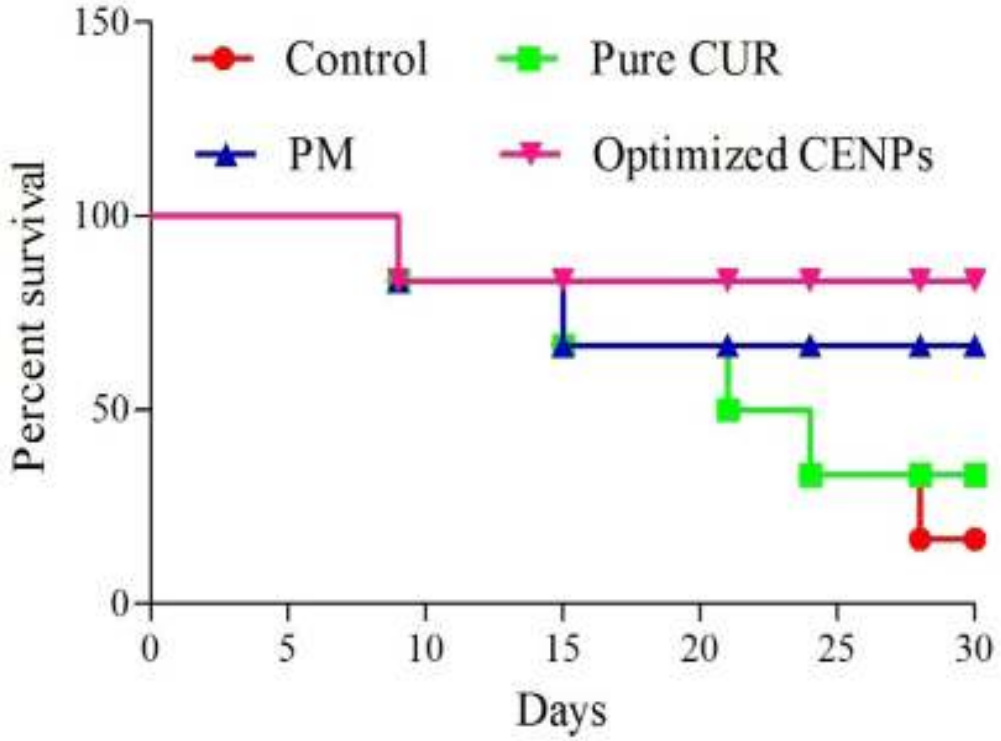

Figure 6.37 Kaplan-Meier survival curve of tumor-bearing mice treated with control and various CUR formulations.

At the end of the treatment, tumors were excised and weighed. The tumor weight of different treatment groups are shown in Figure 6.38.

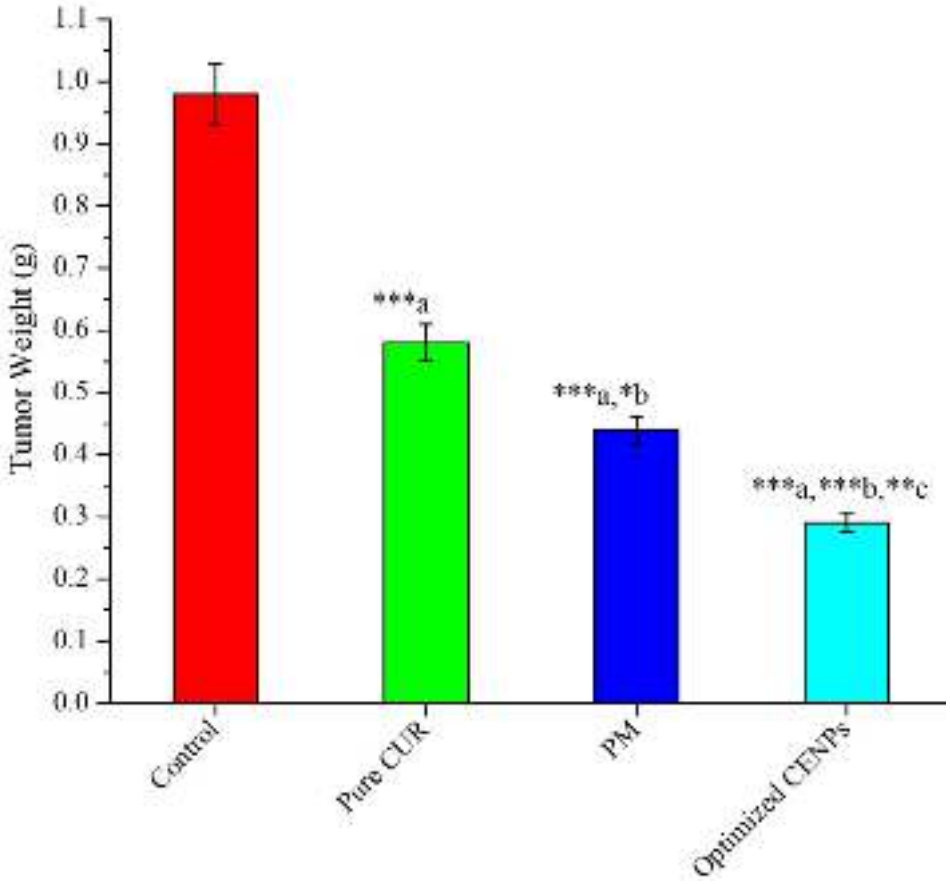

Figure 6.38 Tumor weight of each groups at the end of the test (i.e. after 30 days of dose administration observation);
Vertical bars represent ±SEM; n=6.
(*p<0.001, **p<0.01, *p<0.05 a vs control, b vs pure CUR and c vs PM; One-way ANOVA followed by Tukey's multiple comparison test).**

Above results indicated that, daily oral administration of optimized CENPs for 30 days significantly reduced tumor volume as compared to pure CUR and PM. On the contrary, a continued increase in the tumor volume was observed in control treated group of mice. The enhanced efficacy of optimized CENPs could be attributed to an increased bioavailability of CUR by CENPs. The increased absorption of nanoparticulate carriers through a specific region of the GIT leads to their increased availability in the central compartment (Bhardwaj *et al.,* 2009). Since the optimized CENPs exhibited a sustained release pharmacokinetic pattern, and had a longer circulation time in the blood compartment, it can prevent quick elimination of the drug from the blood circulation and can provide

sufficient time for the greater accumulation of CENPs at the tumor sites. This accumulation at tumor site occur due to the "leaky vasculature" of solid tumor and inflamed tissues having larger pore size that varies between 200 and 780 nm (Torchilin, 2007). Therefore, while pure CUR molecules are typically small enough to permeate out from normal vasculature to be taken up by tissues all over the body, when CUR encapsulated in PNs are retained within the circulatory system because the size of the PNs was greater than the pure CUR. The prepared polymer-based nanosized CUR nanoparticles have a size less than 300 nm in diameter and cannot be cleared by the kidneys but must exit capillaries at sites of leaky microvasculature. Altered circulation of the encapsulated CUR, thus increases CUR accumulation at the targeted tumor or inflammed sites via passive targeting and decreases the drug concentration in normal healthy tissues due to nonavailability of leaky vasculature, thereby potentiating drug (CUR) efficacy in CRC treatment while reducing systemic adverse reactions. This phenomenon is termed as the enhanced permeability and retention (EPR) effect (Acharya & Sahoo, 2001).

Moreover, Kaplan-Meier survival curves showed an enhanced survival time of tumor-bearing mice following oral administration of optimized CENPs as compared to pure CUR and PM. Thus, the anticancer efficacy study of CENPs offered convincing evidence of their enhanced effectiveness as compared to PM and pure CUR for the treatment of CRC.